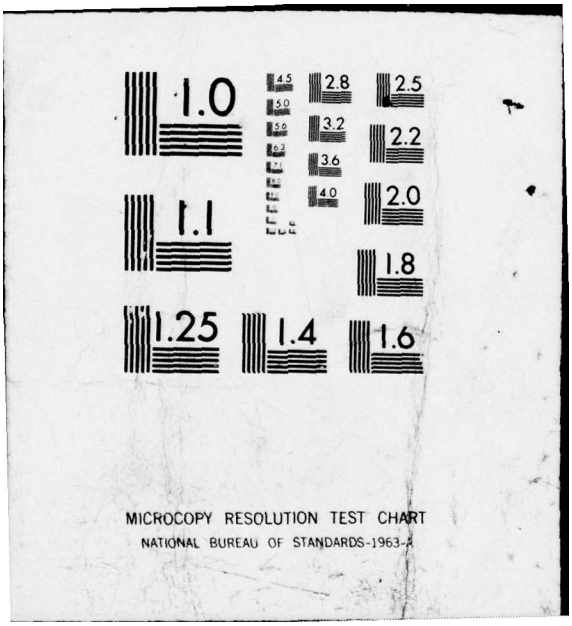
AD-A033 785 GENERAL ELECTRIC CO PHILADELPHIA PA SPACE DIV F/G 9/5
EMP SURGE SUPPRESSION DEVICES UTILIZING METAL OXIDE VARISTORS F--ETC(U)
MAR 76 D M TASCA, S J STOKES, J P QUINE DAAG39-75-C-0008
UNCLASSIFIED 75SDS-4272 HDL-CR-76-008-1 NL

1 OF 2
AD
A033785




1.0
1.1
1.25
1.4
1.6
1.8
2.0
2.2
2.5
2.8
3.2
3.6
4.0
4.5
5.0
5.6
6.3
7.1
MICROCOPY RESOLUTION TEST CHART
NATIONAL BUREAU OF STANDARDS-1963-A

HDL-CR-76-008-1

(12 p.s.)

AD A033785

EMP SURGE SUPPRESSION DEVICES UTILIZING METAL OXIDE VARISTORS FOR HIGH FREQUENCY APPLICATIONS

FINAL TECHNICAL REPORT

MARCH 1976

DDC
RECEIVED
DEC 28 1976
C

Prepared by
General Electric Company
Space Division
Valley Forge Space Center
P. O. Box 8555
Philadelphia, Pa. 19101

Under Contract
DAAG39-75-C-0008
This work was sponsored by the Defense Nuclear Agency
under Subtask R99QAXEB009/42, Work Unit 42



U.S. Army Materiel Command
HARRY DIAMOND LABORATORIES
Adelphi, Maryland 20783

APPROVED FOR PUBLIC RELEASE; DISTRIBUTION UNLIMITED.

HDL-CR-76-008-1, EMP Surge Suppression Devices Utilizing Metal Oxide Varistors for High Frequency Applications, by D. M. Tasca, S. J. S

The findings in this report are not to be construed as an official Department of the Army position unless so designated by other authorized documents.

Citation of manufacturers' or trade names does not constitute an official indorsement or approval of the use thereof.

Destroy this report when it is no longer needed. Do not return it to the originator.

UNCLASSIFIED

SECURITY CLASSIFICATION OF THIS PAGE (When Data Entered)

REPORT DOCUMENTATION PAGE

READ INSTRUCTIONS BEFORE COMPLETING FORM

1. REPORT NUMBER: 75SDS4272	2. GOVT ACCESSION NO.
3. RECIPIENT'S CATALOG NUMBER	
4. TITLE (and Subtitle): EMP SURGE SUPPRESSION DEVICES UTILIZING METAL OXIDE VARISTORS FOR HIGH FREQUENCY APPLICATIONS.	5. TYPE OF REPORT & PERIOD COVERED: FINAL TECHNICAL REPORT. 8/74 - 12/75 - Dec 75
	6. PERFORMING ORG. REPORT NUMBER: 75SDS4272
7. AUTHOR(s): DANTE M. TASCA, SAMUEL J. STOKES III AND JOHN P. QUINE	8. CONTRACT OR GRANT NUMBER(s): DAAG39-75-C-0008 Navy; HDL PROJECT E044E6
9. PERFORMING ORGANIZATION NAME AND ADDRESS: GENERAL ELECTRIC COMPANY, SPACE DIVISION, PHILADELPHIA, PENNSYLVANIA 19101	10. PROGRAM ELEMENT, PROJECT, TASK AREA & WORK UNIT NUMBERS: AMCMS CODE: 691000.22.10922; WORK UNIT: 42
11. CONTROLLING OFFICE NAME AND ADDRESS: DIRECTOR, DEFENSE NUCLEAR AGENCY, WASHINGTON, D.C. 20305	12. REPORT DATE: MARCH 1976
	13. NUMBER OF PAGES: 103
14. MONITORING AGENCY NAME & ADDRESS (if different from Controlling Office): DEPARTMENT OF THE ARMY, HARRY DIAMOND LABORATORIES, 2800 POWDER MILL ROAD, ADELPHI, MARYLAND 20783	15. SECURITY CLASS. (of this report): UNCLASSIFIED
	15a. DECLASSIFICATION/DOWNGRADING SCHEDULE

16. DISTRIBUTION STATEMENT (of this Report)

Approved for public release; distribution unlimited.

HDL CR-76-008-1

17. DISTRIBUTION STATEMENT (of the abstract entered in Block 20, if different from Report)

18. SUPPLEMENTARY NOTES

This work was sponsored by the Defense Nuclear Agency under Subtask R99QAXEB099/42, Work Unit 42.

19. KEY WORDS (Continue on reverse side if necessary and identify by block number)

EMP (ELECTROMAGNETIC PULSE)
TERMINAL PROTECTION DEVICE
METAL OXIDE VARISTOR
HIGH FREQUENCY OPERATION
LOW INSERTION LOSS

20. ABSTRACT (Continue on reverse side if necessary and identify by block number)

This report summarizes the analytical and experimental work performed in developing a surge suppression assembly for high frequency applications utilizing metal oxide varistor materials. The goal of this effort was the development of a terminal protection unit for EMP protection whose insertion losses for normal signal conditions do not exceed 1 db for signal frequencies up to 100 MHz. The development of the desired terminal protection

over

DD FORM 1 JAN 73 1473 EDITION OF 1 NOV 65 IS OBSOLETE

UNCLASSIFIED 405 025

SECURITY CLASSIFICATION OF THIS PAGE (When Data Entered)

unit was investigated using the varistor material in two broad circuit configurations; these being distributed parameter and lumped parameter configurations.

Both the distributed parameter and lumped parameter studies have shown that high frequency, metal oxide varistor terminal protection assemblies are feasible. Parametric design analyses were performed which showed that a modified microstrip line incorporating a ferrite with relative permeability of greater than 16 was an optimum configuration for a distributed parameter assembly. A similar parametric analysis showed that low pass Chebyshev and Constant-K filter configurations represented the optimum for a lumped parameter assembly. A comparison of losses between both configurations also showed that the inherent losses in the distributed and lumped parameter configurations were comparable.

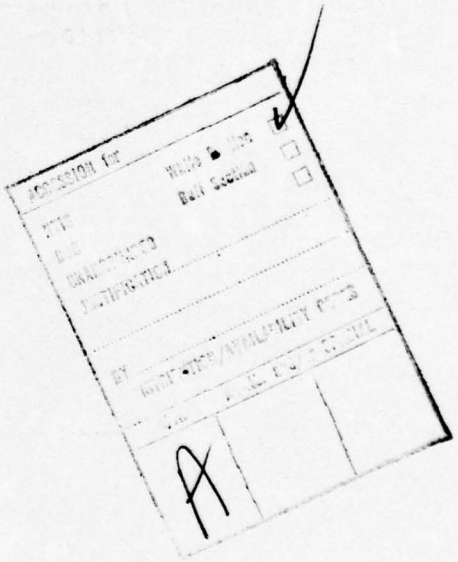
Detailed design equations were developed for a Constant-K filter with microstrip inductors as the baseline configuration. It was shown that minimum insertion loss resulted when using a mismatched filter which also maximized the amount of varistor material in the filter. Design relationships describing the optimum filter characteristic impedance to meet specified insertion loss requirements were also developed. Two prototype filter versions based on this optimum design were developed and fabricated for evaluation. Engineering versions of each filter type were also evaluated under high current pulse stressing and demonstrated that the varistor characteristics are preserved when integrated into the filter configuration.

Some basic performance information on advanced varistor material compositions was also obtained. The material types examined are still in the developmental stages within the General Electric Company. However, they do appear attractive for high frequency terminal protection applications.

FOREWORD

This Final Technical Report was prepared by the General Electric Company, Space Division, Philadelphia, Pennsylvania, under U. S. Army Contract DAAG39-75-C-0008, Defense Nuclear Agency NWED Subtask R99QAXEB099, Work Unit 42, Metal Oxide Varistor Protection Devices. The work was administered under the direction of the U. S. Army, Harry Diamond Laboratories, Electromagnetic Effects Laboratory, 2800 Powder Mill Road, Adelphi, Maryland 20783. Technical monitoring of the contract at USA/HDL was under the direction of A. Renner and J. Kreck. The program manager at General Electric Company was J. C. Peden. The principal investigators were D. M. Tasca and S. J. Stokes, III of the General Electric Company, Space Division, and J. P. Quine of the General Electric Company, Corporate Research and Development Center.

The authors wish to acknowledge the following individuals for their contributions to the work reported here: H. O'Donnell, B. A. Pokol and J. R. Greenwald of the General Electric Company, Space Division, and C. C. Allen, W. A. Davis, R. A. Dehn, I. W. Pence, L. M. Levinson, J. F. Burgess and C. A. Neugebauer of the General Electric Company, Corporate Research and Development Center.



FOREWORD

This Final Technical Report was prepared by the General Electric Company, Space Division, Philadelphia, Pennsylvania, under U. S. Army Contract DAAG39-75-C-0008,Defense Nuclear Agency NWED Subtask R99QAXEB099, Work Unit 42, Metal Oxide Varistor Protection Devices. The work was administered under the direction of the U. S. Army, Harry Diamond Laboratories, Electromagnetic Effects Laboratory, 2800 Powder Mill Road, Adelphi, Maryland 20783. Technical monitoring of the contract at USA/HDL was under the direction of A. Renner and J. Kreck. The program manager at General Electric Company was J. C. Peden. The principal investigators were D. M. Tasca and S. J. Stokes, III of the General Electric Company, Space Division, and J. P. Quine of the General Electric Company, Corporate Research and Development Center.

The authors wish to acknowledge the following individuals for their contributions to the work reported here: H. O'Donnell, B. A. Pokol and J. R. Greenwald of the General Electric Company, Space Division, and C. C. Allen, W. A. Davis, R. A. Dehn, I. W. Pence, L. M. Levinson, J. F. Burgess and C. A. Neugebauer of the General Electric Company, Corporate Research and Development Center.

SUMMARY

The objective of this program was to perform a feasibility study of utilizing metal oxide varistor materials to develop a surge suppression assembly for high frequency applications. The goal of this effort was the development of a terminal protection unit for EMP protection whose insertion losses for normal signal conditions do not exceed 1 db for signal frequencies up to 100 MHz. Clamping voltage requirements were in the range of 100 to 2000 Volts, while the total varistor area was desired to be in the range of 0.1 cm^2 to 1 cm^2 for adequate energy absorption capability. Impedance matching for minimum insertion loss considered only a 50 ohm system in the present study. The terminal protection devices were to be developed using Type DD material, exclusively. Some advanced varistor material evaluations, however, were performed in order to determine their utility for future applications in this area.

The development of the desired terminal protection unit was investigated using the varistor material in two broad circuit configurations; these being distributed parameter and lumped parameter configurations. The distributed parameter studies evaluated the feasibility of achieving the desired insertion loss goal from a distributed parameter approach whereby the metal oxide varistor material is used as part of a signal transmission medium, such as the dielectric material in a coaxial transmission line, whose characteristic impedance is determined by dielectric geometry and dielectric constant. The lumped parameter studies, on the other hand, evaluated the feasibility of achieving the desired insertion loss goal from a lumped parameter approach utilizing the metal oxide varistor as a discrete circuit element or elements. Here, the metal oxide varistor was investigated in tuned circuit and filter type assemblies with the capacitive elements being formed by the varistor material.

Both the distributed parameter and lumped parameter studies have shown that high frequency, metal oxide varistor terminal protection assemblies are feasible. Parametric design analyses were performed which showed that a modified microstrip line incorporating a ferrite with relative permeability of greater than 16 was an optimum configuration for a distributed parameter assembly. A similar parametric analysis showed that low pass Chebyshev and Constant-K filter configurations represented the optimum for a lumped parameter assembly.

Insertion loss analyses for both the distributed parameter and lumped parameter configurations identified the dielectric resistivity of the metal oxide varistor as the prime source of insertion loss. A comparison of losses between both configurations

also showed that the inherent losses in the distributed and lumped parameter configurations were comparable.

Detailed design equations were developed for a Constant-K filter with microstrip inductors as the baseline configuration. It was shown that minimum insertion loss resulted when using a mismatched filter which also maximized the amount of varistor material in the filter. Design relationships describing the optimum filter characteristics impedance to meet specified insertion loss requirements were also developed.

Two prototype filter versions based on this optimum design were developed and fabricated for evaluation. One version utilized 1.8 millimeter thick varistor elements while the other utilized 3.8 millimeter thick varistor elements. The design insertion loss and total filter capacitance was 1.38 db and 267 picofarads. The 1.8 millimeter thick units were measured to be in the range of 3.4 to 4 db and 304 to 344 picofarads, respectively. The 3.8 millimeter thick units were measured to be in the range of 1.6 to 2.7 db and 293 to 311 picofarads. The departure from the design level was not due to the varistor integration concept, but was a result of the increased capacitance incorporated into the filter due to the method used in fabricating the varistor electrodes.

Engineering versions of each filter type were also fabricated for evaluation under high current pulse stressing. Both the 1.8 millimeter and 3.8 millimeter thick varistor filters were exposed to 15 microsecond wide critically damped pulses of 100 to 2500 amperes peak level. The filter output voltage was measured and compared to calculated values using the previously known material characteristics. The close agreement of the experimental and calculated values demonstrated that the varistor characteristics are preserved even when integrated into the filter configuration.

Some basic performance information on advanced varistor material compositions was also obtained. The material types examined were a thick film metal oxide varistor material and the presently so-called "reconstituted" metal oxide varistor material. Both material types are still in the developmental stages within the General Electric Company. However, they do appear attractive for high frequency terminal protection applications. The "reconstituted" varistor material consists of a powdery mixture which can be molded under moderate temperatures to any geometrical configuration desired. The material exhibits an effective dielectric constant of about a factor of thirty less than the standard sintered material and is attractive for applications as a microstrip or filter substrate. The thick film varistor material, as its name implies, can be applied using standard thick film techniques and has potential interest in high frequency, thick film device technology.

TABLE OF CONTENTS

SECTION		PAGE
	Foreword	3
	Summary	5
	List of Figures	8
	List of Tables	11
1	Introduction	13
2	Electrical Characteristics of the Type DD GE-MOV® Varistor	15
3	Evaluation of Metal Oxide Varistors for High Frequency Applications	24
	3.1 Distributed Parameter Configuration	24
	3.2 Lumped Parameter Configuration	54
	3.3 Insertion Loss Comparisons of Distributed and Lumped Parameter Configurations	79
4	Prototype Design and Evaluation	83
5	Advanced Metal Oxide Varistor Material Considerations	95
6	Conclusions	99
7	Recommendations	101
8	References	102

LIST OF FIGURES

FIGURE	TITLE	PAGE
1.	AC Equivalent Circuit of the Type DD GE-MOV^R Varistor Material.	17
2.	AC Dielectric Characteristics of the Type DD GE-MOV^R Varistor Material at Room Temperature (Reference 2).	20
3.	Insertion Loss Characteristics of the Type DD GE-MOV^R Varistor Material in a 50 Ohm System at Room Temperature.	22
4.	Conventional Microstrip Configuration.	26
5.	First Modified Microstrip Configuration.	29
6.	Second Modified Microstrip Configuration.	32
7.	Interconnected Microstrip Lines in a Grooved High-μ Slab.	36
8.	Flat Spiral on Metal Oxide Varistor Configuration.	40
9.	Coaxial Line with Helical Center Conductor.	42
10.	Coaxial Line with Helical Center Conductor (Metal Oxide Varistor Material in Angular Sector <360°).	46
11.	Metal Oxide Varistor and High-μ Discs Cascaded in a Coaxial Line.	47
12.	Equivalent Circuit for the Configuration Shown in Figure 11.	48
13.	Metal Oxide Varistor in Ridge Waveguide Configuration.	51
14.	Capacitance and Loss Characteristics of the Type DD GE-MOV^R Varistor Versus Varistor Area to Thickness Values.	57
15.	Insertion Loss Versus Frequency Characteristics for Various Metal Oxide Varistor Area to Thickness Values.	58

LIST OF FIGURES
(CONTINUED)

FIGURE	TITLE	PAGE
16.	Phase Shift Versus Frequency Characteristics for Various Metal Oxide Varistor Area to Thickness Values.	59
17.	Insertion Loss Due to Dielectric Resistivity Versus Frequency for Various Metal Oxide Varistor Area to Thickness Values.	60
18.	Insertion Loss Characteristics of a Single Stage Metal Oxide Varistor-Parallel Tuned Circuit for the 3 to 30 Megahertz Band.	61
19.	Phase Shift Characteristics of a Single Stage Metal Oxide Varistor-Parallel Tuned Circuit for the 3 to 30 Megahertz Band.	62
20.	Inductance Requirements for a 3 to 30 Megahertz Band, Single Stage Metal Oxide Varistor-Parallel Tuned Circuit.	63
21.	Insertion Loss Characteristics of a Single Stage Metal Oxide Varistor-Parallel Tuned Circuit for the 30 to 70 Megahertz Band.	64
22.	Phase Shift Characteristics of a Single Stage Metal Oxide Varistor-Parallel Tuned Circuit for the 30 to 70 Megahertz Band.	65
23.	Comparison of Lossless Low Pass Filter Types for the Same Total Varistor Capacitance.	66
24.	Single π Section of a Lossy Constant-K Filter.	70
25.	Inductance and 100 Megahertz Q Values for Flat Ribbon Wire.	74
26.	Output Power Characteristics of a Matched and Unmatched Optimally Terminated, Single Section, Lossless Constant-K Filter.	75
27.	Input Impedance Characteristics of a Matched and Unmatched Optimally Terminated, Single Section, Lossless Constant-K Filter.	76

LIST OF FIGURES
(CONTINUED)

FIGURE	TITLE	PAGE
28.	Optimum Termination Impedance to Yield Maximum Varistor Area to Thickness Capability for a Multi-Section Constant-K Varistor Filter (Inductor Q > 100 at 100 Megahertz, Varistor Q = 50).	78
29.	Single π Section of the Prototype Five Stage Constant-K Varistor Filter.	85
30.	Design Insertion Loss of the Prototype Five Stage Constant-K Varistor Filter.	86
31.	Design Phase Shift of the Prototype Five Stage Constant-K Varistor Filter.	87
32.	Fringing Capacitance Effects in Various Metal Oxide Varistor Material Geometries.	89
33.	Engineering Assembly Drawing of the Prototype Five Stage Constant-K Varistor Filter.	90
34.	Insertion Loss Characteristics of Standard Sintered and "Reconstituted" Metal Oxide Varistor Materials.	96
35.	Voltage-Current Characteristics of "Reconstituted" Metal Oxide Varistor Materials.	97
36.	Voltage-Current Characteristics of Thick Film Metal Oxide Varistor Materials.	98

LIST OF TABLES

TABLE	TITLE	PAGE
1.	Voltage-Current Characteristics of the Type DD GE-MOV^R Varistor Material at Room Temperature.	18
2.	High Energy, Pulse Current Effects in the Type DD GE-MOV^R Varistor Material.	23
3.	Z_o and $\sqrt{\epsilon_{EFF}}$ For a Conventional Microstrip Configuration.	27
4.	Calculated Values of Z_o for First Modified Microstrip Configuration.	31
5.	Calculated Values of L_1 and L_2 (nanohenries/meter) for the Second Modified Microstrip Configuration.	34
6.	Characteristic Impedance and Normalized Phase Velocity for the Coaxial Line with a Helical Center Conductor Shown in Figure 9.	43
7.	Total Capacitance and Element Inductance for Various Lossless Low Pass Filter Types With a 30 Megahertz 3 db Frequency.	68
8.	Total Capacitance and Element Inductance Values for Various Lossless Low Pass Filter Types With a 100 Megahertz 3 db Frequency.	69
9.	Insertion Loss Characteristics of the 3.8 Millimeter Thick, Metal Oxide Varistor Filters.	91
10.	Insertion Loss Characteristics of the 1.8 Millimeter Thick, Metal Oxide Varistor Filters.	92
11.	Typical High Pulse Power Voltage-Current Characteristics of the Five Stage Constant-K Varistor Filters.	94

1. Introduction

This document is the Final Technical Report for U.S. Army, Harry Diamond Laboratories Contract DAAG39-75-C-0008, "EMP Surge Suppression Devices Utilizing Metal Oxide Varistors for High Frequency Applications". The objective of the program was to perform a feasibility study of utilizing metal oxide varistor materials to develop a surge suppression assembly for high frequency applications. The goal of this effort was the development of a terminal protection unit for EMP protection whose insertion losses for normal signal conditions do not exceed 1 db for signal frequencies up to 100 MHz. Clamping voltage requirements were in the range of 100 to 2000 Volts, while the total varistor area was desired to be in the range of 0.1 cm^2 to 1 cm^2 for adequate energy absorption capability. Impedance matching for minimum insertion loss considered only a 50 ohm system in the present study. The terminal protection devices were to be developed using type DD material exclusively. Some advanced varistor material evaluations, however, were performed in order to determine their utility for future applications in this area.

The program consisted of four distinct tasks. The first task was to evaluate the development of the desired terminal protection device using the varistor in a distributed parameter configuration, while the second task was to perform a similar evaluation for the varistor in a lumped parameter configuration. The third task was to select the most attractive configuration and develop prototype terminal protection units. The fourth task consisted of a relatively small level of effort with respect to evaluating advanced varistor material compositions for high frequency applications.

The configuration evaluation studies, Task 1 and 2, were concerned with evaluting the varistor material in two broad circuit configurations; these being distributed parameter and lumped parameter configurations. The distributed parameter studies evaluated the feasibility of achieving the desired insertion loss goal from a distributed parameter approach whereby the metal oxide varistor material is used as part of a signal transmission medium, such as the dielectric material in a coaxial transmission line, whose characteristics impedance is determined by dielectric geometry and dielectric constant. The lumped parameter studies, on the other hand, evaluated the feasibility of achieving the desired insertion loss goal from a lumped parameter approach utilizing the metal oxide varistor as a discrete circuit element or elements. Here, the metal oxide varistor was investigated in tuned circuit and filter type assemblies with the capacitive elements being formed by the varistor material.

Task 3 developed prototype terminal protection assemblies in a lumped parameter, 5 stage Constant-K filter configuration. Two versions were fabricated: one with 1.8 millimeter thick varistor units and one with 3.8 millimeter thick varistor units.

The fourth task consisted of obtaining some basic performance information on advanced varistor material compositions. The material types examined consisted of a moderate temperature, moldable powdered material form presently referred to as a "reconstituted" material and a thick film varistor material. The first material type is attractive for achieving microstrip configurations while the latter is attractive for thick film, high frequency device technology.

2. Electrical Characteristics of the Type DD GE-MOV^R Varistor Material

Before discussing the development of the high frequency metal oxide varistor terminal protection assembly, it will be beneficial to briefly review the principle electrical characteristics of the material which control its transient suppression and insertion loss characteristics.

The GE-MOV^R varistor material is basically a ceramic material which offers a unique property of highly non-linear resistance (varistor) and large energy absorbing capability. The varistor, when connected in an electrical circuit, exhibits, over a wide current range, a power law relationship between the current (I) flowing through the material and the voltage (V) across the terminals. This relationship is in the form:

$$I = (V/C)^N$$

where C and N are constants, reflecting composition and geometry parameters, and are primarily a bulk property of the material. The exponent N will typically have values from 25 to 50 or more leading to a characteristic very similar to that of a Zener diode. Older varistor materials by comparison have exponents on the order of 5. Over a wide current range, the voltage remains within a very narrow band for a specific device, and is referred to as the "varistor voltage" for that device. The value of this varistor (or clamping) voltage for a particular device is linearly dependent upon the thickness of the conduction path through the device; the thicker the material, the higher the varistor voltage. The material is bipolar in that the nonlinear resistance characteristic holds for both positive and negative polarity current. Also, the bulk properties of the material provide an inherent high energy absorbing capability, because energy dissipation is evenly distributed throughout the bulk.

The varistor possesses very fast current switching characteristics, being able to switch high current subnanosecond rise time transients without any measurable time delay. Further, its electrical characteristics are a function of material properties and geometrical shape. As noted previously, the clamping voltage is a direct linear function of thickness of the material between the conduction electrodes. Because of this geometrical dependence, the application of this material as a transient protection device is quite flexible in achieving optimum configurations. The material can be readily pressed, sliced, machined, etc., into a variety of shapes; such as cylinders, disks, doughnuts, squares, and so forth, and still maintain desirable electrical characteristics.

The varistor characteristics presented below consist of a

summary of the detailed measurements previously obtained under contract DAAG39-72-C-0179 (Reference 1) together with the results of recent internal General Electric Company measurements (Reference 2) describing the detailed frequency dependent, dielectric behaviour of the varistor material. The information is presented in terms of geometry independent material parameters rather than absolute values related to specific geometrical configurations. In this way, one can perform a parametric analysis to select the optimum geometrical configuration to satisfy a specific application from the definition of the quiescent bias, clamping voltage, pulse energy threat and insertion loss requirements. For brevity, the data summary is presented in terms of the characteristics associated with the standard type "DD" material fabricated by the General Electric Company, Semiconductor Products Department, since it was the only material type considered in the present study.

2.1 A. C. Equivalent Circuit

A suitable equivalent circuit which describes the electrical operation of the varistor material for AC conditions is shown in Figure 1. The circuit consists of the parallel combination of a capacitance (due to the very thin dielectric of the intergranular phase), a high resistance leakage resistor (attributable to the high resistivity of the bismuth oxide in the intergranular phase), and a nonlinear conduction element-varistor element-(associated with the intergranular phase) in series with a low resistance series resistor (due to the low resistivity of the zinc oxide grains). Any application of wire leads, etc., to the material would, of course, result in an addition of a series inductance to the equivalent circuit in a manner similar to that associated with other electronic devices.

The bulk conduction properties of the varistor material are manifested in the V-I relationship for the varistor element shown in Figure 1. As indicated, the voltage drop across the element is linearly related to the thickness, "L", of varistor material between conducting electrodes and the current density (current "I" and cross-sectional area "A") through the material. The coefficient of nonlinearity, "N", typically has values on the order of 25 to 50. The parallel resistance and capacitance are frequency dependent and is further discussed in Section 2.3.

2.2 Voltage-Current Characteristics

The voltage-current characteristics of the type DD varistor material is shown in Table 1 (Reference 1) for a 25°C ambient temperature. The varistor characteristics are given for a range of over eleven orders of magnitude in operating current density. Shown here is the relationship of the voltage drop per millimeter of material

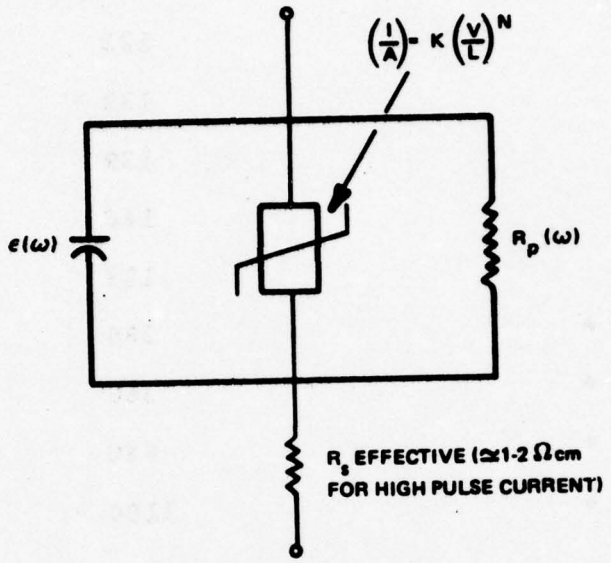


Figure 1. AC Equivalent Circuit of the Type DD GE-MOV^R Varistor Material.

TABLE 1. Voltage-Current Characteristics of the Type DD GE-MOV^{R} Varistor Material at Room Temperature

CURRENT DENSITY (AMPERES/CM^2)	AVERAGE VOLTS/MM THICKNESS
8×10^{-8}	111
8×10^{-7}	123
8×10^{-6}	132
8×10^{-5}	139
8×10^{-4}	146
8×10^{-3}	153
8×10^{1} *	280
8×10^{2} *	360
8×10^{3} *	640
3×10^{4} *	1100

* PULSE MEASUREMENTS

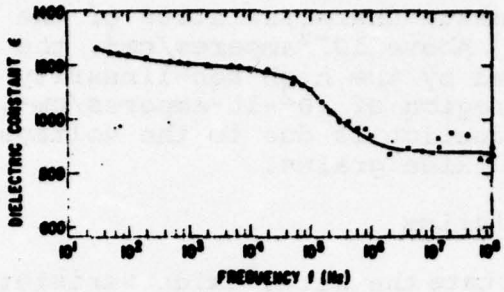
thickness to the amperes per square centimeter current density operating level for the varistor material. D.C. measurements were used to obtain the varistor characteristics for current densities less than 10 milliamperes/cm^2. Higher current density characteristics were obtained from pulse measurements.

Below about 10^{-8}amperes/cm^2, the conduction characteristics are controlled by the leakage characteristics of the high resistivity bismuth oxide insulator. Above 10^{-8}amperes/cm^2, the conduction characteristics are controlled by the high non-linearity of the intergranular phase. In the region of 10^2-10^3amperes/cm^2, the departure from high non-linear conduction is due to the voltage drop across the low resistivity zinc oxide grains.

2.3 Dielectric Characteristics

In the unenergized state the metal oxide varistor is essentially a ceramic material which is primarily capacitive due to the dielectric nature of the intergranular phase. Levinson and Philipp (Reference 2) have recently completed a detailed evaluation of the dielectric behaviour of the metal oxide varistor over a frequency range from 10 Hz to greater than 100 MHz. Their results, which are given in Figure 2, show that the dielectric constant and loss are both frequency dependent. At 100 MHz the varistor material has a dielectric constant of 875 and a Q of 50. The Q is somewhat constant with frequency, exhibiting a minimum of 10 at 250 KHZ.

It should be noted that, in evaluating the dielectric constant of a material, a common procedure is to perform impedance or reflection coefficient (ρ) measurements on standard geometrical shapes such as parallel plate or coaxial configurations. These measurements are then related back to the sample geometry to define the dielectric constant of the material. Measurements such as these when applied to the GE-MOV® varistor yield an "effective" or "observed" value of dielectric constant when related to the overall varistor geometry rather than the intergranular phase which is the source of the dielectric nature of the material. This is due to the fact that the overall geometry is composed primarily of conducting zinc oxide grains of approximately 10 microns diameter whereas an upper limit on the size of the intergranular phase in the type "DD" material is estimated at 1000 Angstroms thickness resulting in an actual value for the dielectric constant of the intergranular phase in the type DD material at about two orders of magnitude less than that shown in Figure 2, (Reference 3). However, the effective dielectric characteristics given in Figure 2 are those values which, when used with the total material geometry, yield the appropriate value for the material capacitance and loss.



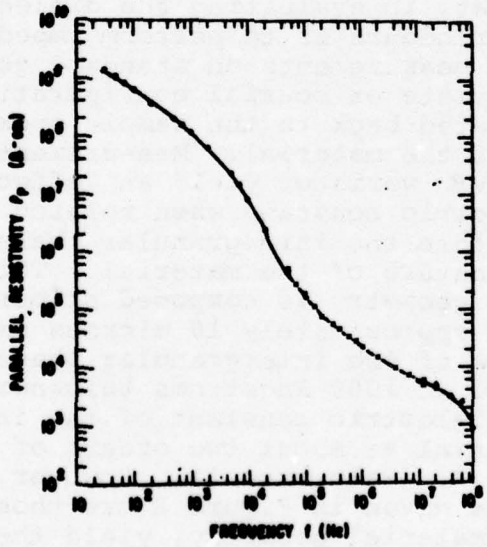


Figure 2. AC Dielectric Characteristics of the Type DD GE-MOV^R Varistor Material at Room Temperature (Reference 2).

2.4 Insertion Loss

Since the insertion loss characteristics of the varistor are related to its dielectric nature, the extent of these effects can be determined from the dielectric constant and loss characteristics of the material. Specific values of capacitance and loss can be determined from a knowledge of the particular geometrical configuration being employed. In the simplest case, neglecting fringing effects, the metal oxide varistor can be considered as a parallel plate capacitor, whose capacitance is portional to the area to thickness ratio and whose loss is proportional to its thickness to area ratio. As such, the capacitance and loss can be defined in terms of geometry independent quantities, and the insertion loss characteristics for a particular impedance system can be determined.

Figure 3 shows the results of one such parametric analysis for a 50 ohm system. The insertion loss characteristics are defined in terms of the maximum area to length ratio which can be used before incurring a 1 db and 3 db insertion loss. The characteristics, which are labeled "capacitive and resistive loss", are those which result from applying the varistor material directly across a circuit at a single node without any frequency compensation. The characteristics labeled "resistive loss", on the other hand, represent the theoretical maximum achievable varistor capability assuming a 100% efficiency in tuning out the capacitive effects. Here, the dielectric loss is the limiting item in achieving low insertion loss characteristics.

2.5 High Energy Absorption Capability

A critical parameter of a protection device is its ability to absorb, or bypass, the unwanted transient energy without suffering significant degradation or damage. In this regard, the GE-MOV^{R} varistor does not exhibit a catastrophic failure threshold as does, say a semiconductor device due to junction burnout. Instead, the varistor will experience a gradual degradation in its low current conduction characteristics for increasing levels of input energy pulses whose deposited energy is sufficient to cause a significant temperature rise in the varistor material.

The pulse energy absorption capability of the type DD varistor material is summarized in Table 2, (Reference 1). The characteristics shown are given in terms of the peak pulse current density which, when passed through the varistor material, result in the indicated quiescent leakage currents when the varistor is biased at 50% of its turn-on voltage level of 150 volts/millimeter thickness.

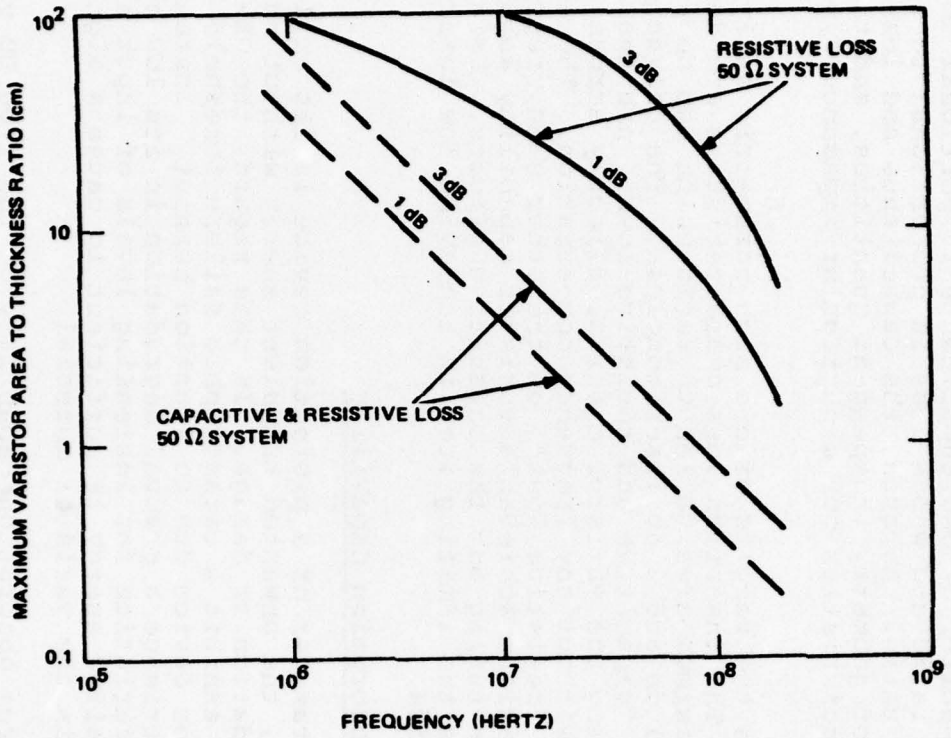


Figure 3. Insertion Loss Characteristics of the Type DD GE-MOV^R Varistor Material in a 50 Ohm System at Room Temperature.

TABLE 2. High Energy, Pulse Current Effects in the Type DD GE-MOV® Varistor Material

PULSE WIDTH (μ Sec)*	PEAK PULSE CURRENT (Amperes/cm^2)	LEAKAGE CURRENT (Amperes/cm^2) AT A 50% VARISTOR VOLTAGE BIAS OF 75 V/MM THICKNESS
1.5	5200	8×10^{-6}
	6400	8×10^{-5}
	13000	8×10^{-4}
	26000	8×10^{-3}
15	5200	8×10^{-6}
	6400	8×10^{-5}
	13000	8×10^{-4}
	16000	8×10^{-3}
150	2600	8×10^{-6}
	3200	8×10^{-5}
	5200	8×10^{-4}
	6400	8×10^{-3}

* FULL WIDTH, 10% LEVEL OF A CRITICALLY DAMPED PULSE SHAPE

3. Evaluation of Metal Oxide Varistors for High Frequency Applications.

As previously indicated, the objective of the present work was to carry out a feasibility study of utilizing metal oxide varistor (MOV) materials to develop a surge suppression assembly for high frequency applications. The goal of this effort was the development of a terminal protection unit for EMP protection whose insertion losses for normal signal conditions do not exceed 1 db for signal frequencies up to 100 MHz. Clamping voltage requirements were in the range of 100 to 2000 Volts, while the total varistor area was desired to be in the range of 0.1 cm^2 to 1 cm^2 for adequate energy absorbtion capability. Impedance matching for minimum insertion loss considered only a 50 ohm system in the present study. The metal oxide varistor material which was evaluated was restricted to the medium voltage material type DD.

The development of the desired terminal protection unit was investigated using the varistor material in two broad circuit configurations; these being distributed parameter and lumped parameter configurations. The distributed parameter studies evaluated the feasibility of achieving the desired insertion loss goal from a distributed parameter approach whereby the metal oxide varistor material is used as part of a signal transmission medium, such as the dielectric material in a coaxial transmission line, whose characteristic impedance is determined by dielectric geometry and dielectric constant. The lumped parameter studies, on the other hand, evaluated the feasibility of achieving the desired insertion loss goal from a lumped parameter approach utilizing the metal oxide varistor as a discrete circuit element or elements. Here, the metal oxide varistor was investigated in tuned circuit and filter type assemblies with the capacitive elements being formed by the varistor material.

Both the distributed parameter and lumped parameter studies are discussed in detail below. A comparison of the losses associated with each approach is also presented.

3.1 Distributed Parameter Configuration

The principle design problem to be solved in integrating the varistor material into a distributed parameter configuration is associated with the high value of the permitivity of the varistor material. This causes the impedance levels of transmission lines to become impractically small. As such, the main design effort centered on evaluating methods for increasing the characteristic impedance by increasing the inductance per unit length of a transmission medium through the use of high permeability material and mutual inductance. A wide range of transmission line configurations

were considered during the study. Among those which were investigated in varying degrees of detail were:

1. Microstrip Configurations
2. Slot and Coplanar Lines
3. Flat Spiral Printed on MOV
4. Coaxial Lines with Helical Center Conductor
5. Cascaded Discs of MOV and High-Permeability Material in Coaxial Line

All of the above configurations are discussed in the following subsections of this report with the exception of the slot and coplanar lines. These were not considered in much detail since they do not differ essentially from a microstrip line as far as the present application is concerned. A possible disadvantage of the slot and coplanar lines is the non-uniform current densities in the MOV material which results from the orientation of the conductors. A microstrip line is nearly ideal in this sense in that the electric field is more nearly constant in the MOV material and results in a more nearly uniform current density and dissipation in the high current state. The ridge-waveguide high pass filter is not considered a promising configuration, and is discussed only for the sake of completeness.

3.1.1 Microstrip Configurations

Figure 4 shows a conventional microstrip configuration which will be considered first. In the present application, the permeabilities correspond to vacuum; i.e., $\mu_1 = \mu_2 = 4\pi \times 10^{-7}$ Henries per meter. The permitivity, ε_2, also corresponds to vacuum and is equal to 8.854×10^{-12} Farads per meter. The relative permitivity, ε_{r1} of the MOV is in the range between 875 and 1200. In this case, the absolute permitivity is given by $\varepsilon_1 = \varepsilon_{r1} \times 8.854 \times 10^{-12}$ Farads per meter.

At low frequencies, the characteristic impedance, Z_o, and wavelength, λ, of the microstrip configuration of Figure 4 depend only on the ratio of strip width w to substrate thickness h. Calculations were performed to determine the value of w/h required to obtain a value of 50 ohms for the characteristic impedance, Z_o. Table 3 lists values of Z_o and effective index of refraction equal to the square root of the effective relative dielectric constant, $(\varepsilon_{EFF})_1$ as a function of the ratio w/h.

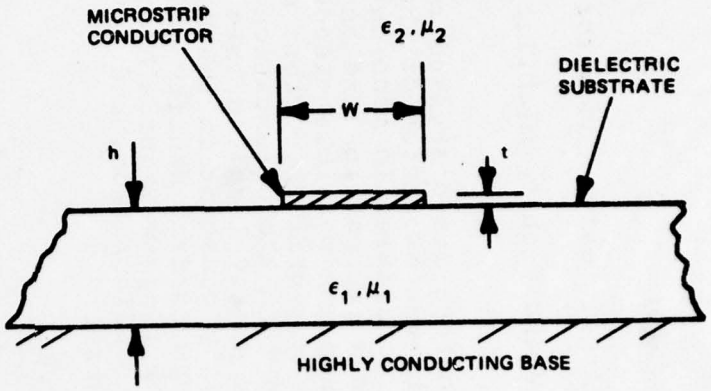


Figure 4. Conventional Microstrip Configuration.

TABLE 3. Z_o and $\sqrt{\varepsilon_{EFF}}$ for a Conventional Microstrip Configuration

$\varepsilon_{r1} = 1000$

$\mu_{r1} = 1$

$t = 0$

w/h	Z_o (OHMS)	$\sqrt{(\varepsilon_{EFF})_1}$
1.000	4.962	25.517
0.100	11.210	23.456
0.010	17.652	22.722
0.001	23.984	22.483
0.0001	30.231	22.407
0.00001	36.436	22.383

Examination of the data presented in Table 3 shows that extremely small values of w/h are needed in order to achieve a value of 50 ohms for Z_o. For small values of w/h, accurate values of Z_o and $\sqrt{(\varepsilon_{EFF})_1}$ are given by

$$Z_o = \frac{60\ \ell n\left(\frac{8h}{w}\right)}{\sqrt{(\varepsilon_{EFF})_1}} \qquad (1)$$

$$(\varepsilon_{EFF})_1 = \frac{\varepsilon_{r1} + 1}{2} \qquad (2)$$

Note that (1) corresponds to the equation for an open-wire line*, while (2) shows that the effective dielectric constant is equal to the average for the two media. Equations (1) and (2) for the limiting values of Z_o and $(\varepsilon_{EFF})_1$ for a microstrip line having small w/h do not appear to be well known. In the other limit, w/h>>10, it is well known, of course, that

$$Z_o = (h/w)\sqrt{\mu_1/\varepsilon_1} \text{ and } (\varepsilon_{EFF})_1 = \varepsilon_1.$$

The conclusion that extremely small values of w/h are required to obtain a value of 50 ohms for Z_o using a conventional microstrip configuration led to a consideration of modified microstrip configurations. The first modified form considered is shown in Figure 5. In this case, the dielectric material is removed from everywhere except directly under the microstrip conductor. This has the effect of decreasing the capacitance per unit length of the microstrip line, while having essentially no effect on the inductance per unit length.

An approximate value for Z_o for the configuration of Figure 5 can be obtained by employing the same value of inductance per unit length as for the configuration of Figure 4 and by employing a modified value for the capacitance per unit length. In this case,

*For a round wire of diameter w at a distance h over a ground plane in free space $Z_o = 60\ell n\left(\frac{4h}{w}\right)$. But since a strip of width w is equivalent to a round wire of diameter w/2, the equivalence of (1) with the well-known expression for an open-wire line is clear.

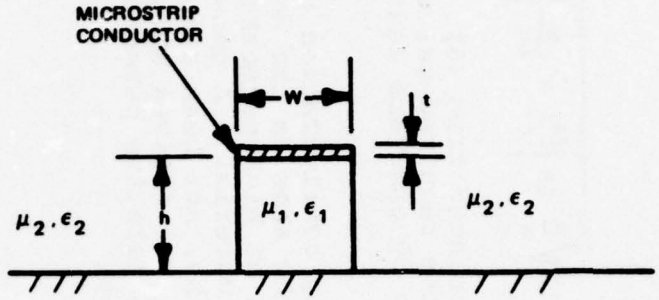


Figure 5. First Modified Microstrip Configuration.

$$L = 2.0\ \ell n\left(\frac{8h}{w} + \frac{w}{4h}\right) \times 10^{-8}\ \text{Henries/meter} \quad (3)$$

$$C = (\varepsilon_{r1}\ w/h) \times 8.854 \times 10^{-12}\ \text{Farads/meter} \quad (4)$$

For $\varepsilon_r = 1000$

$$Z_o = \sqrt{\frac{L}{C}} = 1.503\sqrt{\frac{h}{w}\ \ell n\left[\frac{8h}{w} + \frac{w}{4h}\right]}\ \text{ohms} \quad (5)$$

Table 4 lists values for Z_o calculated from (5). Examination of the data in Table 4 shows that the required values of w/h for obtaining a value of Z_o equal to 50 ohms are again too small to be practical.

The final modified microstrip configuration that was considered is shown in Figure 6. This is the same as the configuration of Figure 5, except that a material of high permeability is employed in region 2 surrounding the MOV material. A general analysis to obtain calculated values for Z_o has not been attempted. However, a simple exact expression for Z_o was derived which is valid in the limit of very high values of the relative permeability μ_{r2}; of the surrounding medium. In this case,

$$Z_o = \sqrt{\frac{\mu_1}{\varepsilon_1}}\ \frac{h}{w} \quad (6)$$

Thus, when the value of μ_{r2} is very high, the field distribution within the MOV is essentially the same as the fields between infinitely conducting parallel plates of infinite width, w, and spaced a distance ,h ,with MOV material placed between the plates.
For $\varepsilon_{r1} = 1000$

$$Z_o = \frac{120}{\sqrt{1000}}\ \frac{h}{w} \quad (7)$$

If a value of 50 ohms is desired for Z_o, the required value of w/h is given by

TABLE 4. Calculated Values of Z_o for First Modified Microstrip Configuration

$\varepsilon_{r1} = 1000$

$\mu_{r1} = 1.0$

$t = 0$

w/h	Z_o
0.010	38.860
0.005	57.735
0.0025	85.399
0.00125	125.851
0.00100	142.486

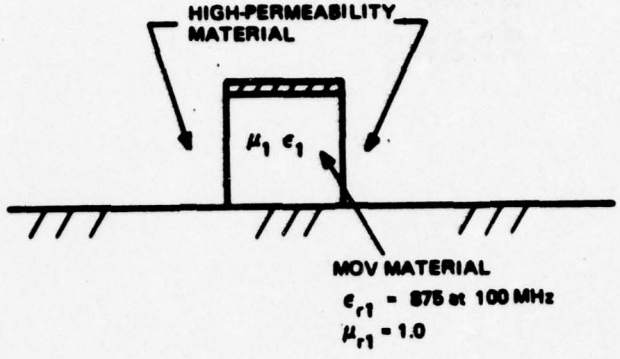


Figure 6. Second Modified Microstrip Configuration.

$$w/h = \frac{120\ \pi}{50\ \sqrt{1000}} = 0.238 \qquad (7a)$$

The minimum value of h is established by the requirement that the minimum clamping voltage be 100 volts. In this case, h = 0.065cm, and the minimum value of w is 0.0155cm or 0.0061 inches. This value of w applies for a value of μ_{r2} which is very much greater than 1.0.

One can obtain an estimate of the required value of μ_{r2} by comparing the inductance L_1 of the completely homogeneous configuration ($\mu_1=\mu_2$) and the inductance L_2 of the inhomogeneous configuration having $\mu_1 = \mu_o = 4\pi \times 10^{-7}$ Henries per meter and μ_2 equal to infinity. The inductance L_2 is therefore the inductance of the "gap" underneath the microstrip conductor filled with MOV material and having $\mu_1 = \mu_o$. If μ_2 is made large enough to cause L_1 to be much greater than L_2, then the inductance L of the actual configuration having $\mu_1 = \mu_o$ and a finite μ_2 will be less than L_2 by only a small amount. The actual inductance, L, has not been calculated rigorously. However, it is believed that in the limit of small values of w/h, the value of L is somewhat greater than the parallel combination of L_1 and L_2. Thus,

$$L > (L_1L_2)/(L_1 + L_2) = L_2\left(\frac{L_1/L_2}{1 + L_1/L_2}\right) \qquad (8)$$

where L_1 and L_2 were defined above and are given by

$$L_1 = 20\ \mu_{r2} \times 10^{-8} \ell n \left(\frac{8h}{w} + \frac{w}{4h}\right) \qquad (9)$$

$$L_2 = 4\pi\ \frac{h}{w} \times 10^{-7} \qquad (10)$$

The units for L_1 and L_2 in (9) and (10) are Henries per meter.

Table 5 shows calculated values of L_1/μ_{r2}, L_2 and the ratio $(L_1/\mu_{r2})/L_2$. Since L_1 is directly proportional to μ_{r2}, it is convenient to present the data in this way. Examination of the data shows that if μ_{r2} is equal to 10 then the ratio L_1/L_2 has a value of 6.99 if h/w is equal to 0.25 which is close to the required value calculated above. From this it is concluded that μ_{r2} should have a minimum value of 10 and preferrably should have a value perhaps as high as 20.

The characteristic impedance, Z_o, decreases somewhat with finite values of the thickness, t, of the microstrip conductor and for finite values of the permeability, μ_{r2}, of the surrounding medium. For this reason a value of w = 0.005" may be more appropriate than the value of 0.0061" calculated above.

TABLE 5. Calculated Values of L_1 and L_2 (nanohenries/meter) for the Second Modified Microstrip Configuration

$t = 0$

h/w	L_1/μ_{r2}	L_2(GAP)	$L_1/L_2/\mu_{r2}$
0.05	337.28	62.83	5.358
0.10	238.78	125.66	1.900
0.15	210.63	188.50	1.117
0.20	209.46	251.33	0.833
0.25	219.72	314.16	0.699
0.30	234.70	376.99	0.623
0.35	251.37	439.82	0.572
0.40	268.31	502.66	0.534
0.45	284.89	565.49	0.504
0.50	300.82	628.32	0.479

Figure 7 shows a method for obtaining the required total length of microstrip line to give 1cm^2 of MOV conducting area (e.g., 78.74cm for the example given above). In this case, several microstrip lines are employed and are interconnected in series as shown. The individual lines can be metalized and placed in grooves in the high-μ slab. Alternately, a high-μ cylinder can be employed containing longitudinal grooves. The values of w, h and t are the same as discussed previously for the single microstrip line of Figure 6. The line spacing S in Figure 7 should be large enough (perhaps S = 10h) to prevent mutual coupling between lines. Mutual coupling would have an effect on the transmission characteristics at high frequencies because of the phase shift between adjacent lines.

Another possibility is to cut the grooves in the shape of a helix on a high-μ cylinder. If the bottom of the grooves are first metalized, the MOV material can then be potted into the grooves. In this case, also, the spacing S between the adjacent turns of the helix should be on this order of 10h to prevent mutual coupling. In this sense, there is an essential difference between the helical-groove configuration described here and the coaxial line with helical center conductor described in Section 3.1.3.

Calculations were also made to determine the temperature rise that can be expected to occur in the microstrip conductor shown in Figure 6 under conditions of a high-current pulse. Neglecting all heat losses due to thermal conduction through the MOV and surrounding material of high permeability, the temperature rises linearly during the pulse at a rate determined by the specific heat of the microstrip conductor and the heat generation rate within the conductor. The temperature rise ΔT under these conditions is given by

$$\Delta T = \frac{Q}{mS} \tag{11}$$

where Q is the generated heat in gm-calories, m is the mass in gms, and S is the specific heat of the microstrip conductor in calories per degree centigrade.

$$Q = \frac{I^2 R_s \Delta t}{4.18605} \tag{12}$$

$$R_s = \rho \, \ell / A \tag{13}$$

$$m = \delta \, A \, \ell \tag{14}$$

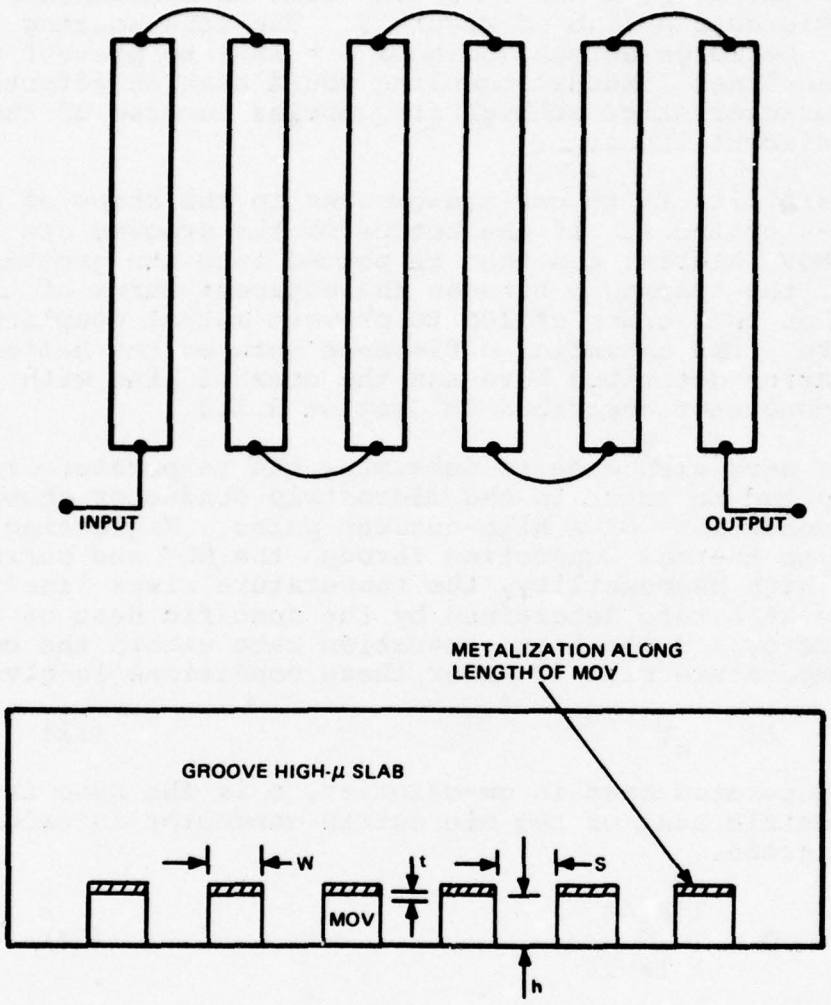


Figure 7. Interconnected Microstrip Lines in a Grooved High-μ Slab.

In the above relations, I is the pulse current, Δt the pulse width, ρ the resistivity, δ the density, ℓ the length and A the cross sectional area of the microstrip conductor. Substituting (12), (13), and (14) into (11) results in

$$\Delta T(°C) = \frac{I^2 \rho \Delta t}{4.18605 A^2 \delta S} \qquad (15)$$

For a microstrip conductor having 0.005" x 0.002" cross section, $A = 64.54 \times 10^{-6} cm^2$. For copper $\rho = 1.7241 \times 10^{-6}$ ohm-cm, $\delta = 8.9$ gms per cubic cm, and the specific heat is 0.093. If the pulse width is 100 microseconds and the pulse current is 100 amperes, the temperature rise ΔT calculated from (15) is 119.5 degrees centigrade. The actual temperature rise will be less than this as a result of heat conduction away from the microstrip conductor. The effect of thermal conduction can be accounted for in a simple manner using a model which applies accurately for the present case, (Reference 5).

The attenuation constant, α, due to loss in the metal for the configuration of Figure 6 (assuming a high value of μ_{r2}) can be calculated from the following formula.

$$\alpha = [R_s/(\eta h)] \times 8.686 \text{ dB/unit length} \qquad (16a)$$

where

$$R_s = 2.61 \times 10^{-7} \sqrt{f} \text{ ohms for copper} \qquad (16b)$$

$$\eta = 120\pi / \sqrt{\varepsilon_{r1}} \qquad (16c)$$

If values of h = 0.065cm and f = 100 MHz are assumed (clamping voltage = 100), the value of α due to finite conductivity of the microstrip conductor calculated from (16a) is 0.0292 dB/cm. It is seen that this alone would yield 2.299 dB at 100 MHz if a length of 78.74 cm is employed corresponding to a conduction area of 1.0 cm^2 with a microstrip width of 0.005".

The dielectric losses occur predominantly as a result of the dielectric losses within the MOV material, the dielectric losses in the high-μ material being small in comparison. Since the dielectric constant of the MOV material is considerably higher than in the surrounding ferrite material, it can be assumed that the electric field within the MOV is nearly uniform. Use of the high-μ material to surround the MOV material also makes the magnetic field nearly uniform within the MOV. The result is that the propagation within the MOV material of finite cross-section is similar to that for an MOV medium of infinite cross-section. In this case the attenuation constant is given by

$$\alpha = \frac{\pi}{\lambda_o} \sqrt{\varepsilon_r \mu_r} \tan \delta \times 8.686 \text{ db/unit length} \quad (17)$$

where ε_r, μ_r and the tan δ are the relative permitivity, relative permeability and loss tangent of the MOV material, and λ_o is the wavelength in vacuum. For the medium-voltage type DD material (Reference 2), $\varepsilon_{r1} \approx 1000$ and tan $\delta \approx 0.002$. Furthermore, for f = 100 MHz, λ_o = 300cm. Under these conditions, the value of α calculated from (17) is 0.0575 dB/cm, which is considerably higher than the attenuations constant due to the finite conductivity of the microstrip conductor alone.

A rigorous expression for the losses due to the ferrite material has not been derived. In this case, the calculation is complicated by the fact that the ferrite does not fill the entire cross-section of the microstrip. However, it is believed that the attenuation constant due to the ferrite material losses will be much less than that due to MOV dielectric losses. For example, Indiana General has material "Q-3" which is characterized by a value of $\mu_r \approx 16$ and a loss tangent of 0.006 at 100 MHz. The value of α for an infinite medium of the material is also given by (17). Since the value of ε_r is on the order of 10 the value of α is 0.0069 dB.cm.* Assuming that the value of α = 0.0069 applies for the ferrite losses, the total attenuation α_T due to microstrip conductor losses (α = 0.0292 dB/cm), MOV dielectric losses (α = 0.0575 dB/cm), and ferrite losses (α = 0.0069 dB/cm) is equal to 0.0936 dB/cm at 100 MHz. From this, one concludes that in order to obtain a total loss of 1.0 dB at 100 MHz the total length of the microstrip line (h = 0.026" for 100 volts w = 0.005" for 50 Ω) should not exceed 10.68cm, and in this case, the conduction area would be 0.1357cm^2.

Only the losses due to finite conductivity of the microstrip conductor depend strongly on the cross-sectional dimensions. Furthermore, since these losses are only a small part of the total losses, it is seen that the value of α is relatively independent of the cross-sectional dimensions, decreasing somewhat with increased cross-sectional dimensions due to a decrease in conductor losses. On the basis, it is seen that one must increase the conductor width w in order to obtain the same area A in a shorter length ℓ = A/w. Thus,

$$\alpha_T \ell = \alpha_T A/w = \alpha_T A(h/w)/h \quad (18)$$

* However, since the magnetic field intensity H within the high-μ material is much less than the value of H within the MOV material, it is concluded that the actual value of α due to ferrite losses is probably much less than the value of α for an infinite medium. It is estimated that the effective loss tangent is roughly (L_2/L_1) tan δ where (L_2/L_1) is obtained from Table 5.

The ferrite saturation current I_s has also been calculated for the configuration of Figure 6. In this case the saturation magnetic field intensity H_s in the MOV material is I_s/w and the saturation flux density B_s is $\mu_o I_s/w$. Since the normal magnetic field is continuous at a boundary, this is also the flux density in the ferrite material just adjacent to the MOV. The Indiana General "Q-3" material has a saturation flux density of 2600 Gauss equal to 2600×10^{-4} Webers/m^2. Therefore, I_s is $B_s\, w/\mu_o$ = 26 amperes, if w = 0.005/39.37 meters and $\mu_o = 4\pi \times 10^{-7}$ Henries/meter. This allows considerable CW power to be transmitted in the normal operating mode before ferrite saturation is encountered.

3.1.2 Flat Spiral on Varistor Material

This configuration is shown in Figure 8. A spiral microstrip conductor is employed in order to obtain an increase in inductance through the mechanism of "mutual inductance". High permeability material is placed all around the MOV material in order to "trap" the magnetic flux within the MOV material. Thus, the MOV material is shaped in the form of a square (or round) annulus. Under these conditions, the magnetic field H is nearly constant within the MOV material, and the inductance per unit length is roughly equal to the inductance per unit length of the microstrip configuration of Figure 6. From another point of view it can be argued that the characteristic impedance for a cell of width W is nearly the same as that for a cell of width w in a parallel-plate-transmission line. Thus, neglecting the small gap G,

$$Z_o = \frac{\mu_1}{\epsilon_1} \frac{h}{w} \qquad (19)$$

which is the same as (6). Thus, all the analytical results derived for the configuration of Figure 6 apply approximately for the configuration of Figure 8. In this connection, the required strip width w to obtain a desired value of Z_o with the configuration of Figure 8 is approximately the same but is somewhat less than that of Figure 6.

The transmission characteristics for the spiral line of Figure 8 should be essentially the same as for the single straight microstrip line of figure 6, provided the phase shift between adjacent conductors is negligible. The phase shift per unit length, β, is given by

$$\beta = \sqrt{\mu_o \epsilon_1} \qquad (20)$$

If f = 100 MHz and ϵ_{r1} = 1000, the value of β calculated from (20) is 37.9 degrees per cm.

Recalling from Section 3.1.1 that a 100 volt clamping voltage and 1 cm^2 MOV conducting area requires 78.74 cm of transmission length, it appears that a spiral configuration having transmission characteristics which are flat out to 100 MHz does not appear practical.

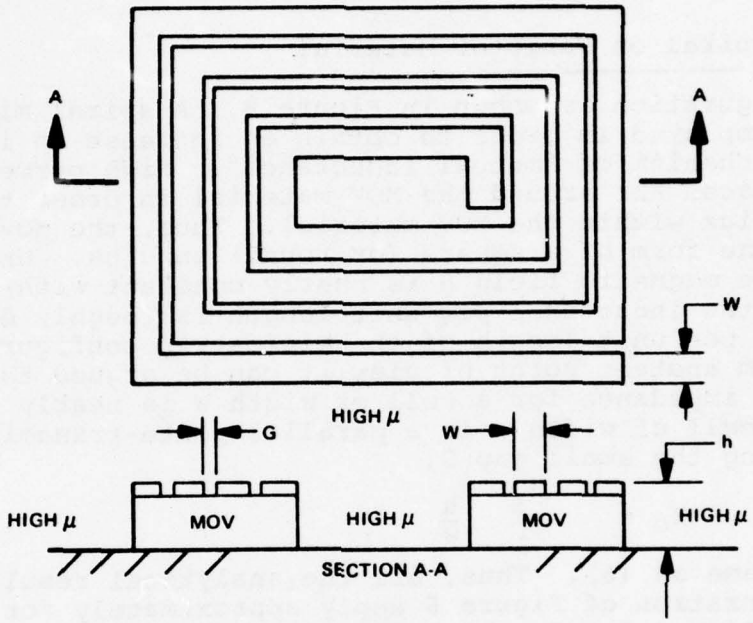


Figure 8. Flat Spiral on Metal Oxide Varistor Configuration.

3.1.3 Coaxial Line With a Helical Center Conductor

A coaxial line with a helical center conductor was also evaluated as a means of obtaining an increased inductance per unit length and therefore a wide strip width, w, for a specified value of Z_o. This configuration is shown in Figure 9. An expression was derived for the characteristic impedance for this configuration. This is given below in (21), and is somewhat more general than (3) given by Winkler in reference 6. References 7 and 8 also treat the same problem. However, in Reference 8, a factor of ε_r is missing in Equation (3) and $\sqrt{\varepsilon}$ is missing in Equation (4); furthermore, the quantity T is defined incorrectly in Equation (9).

$$Z_o = \sqrt{\frac{\mu_1\mu_2 N^2}{8\varepsilon_1} \quad \frac{(a^2-d^2)d^2}{\mu_1(a^2-d^2) + \mu_2 d^2}} \; \ell n \, \frac{a}{d} \tag{21}$$

In (21) N is the number of turns per unit length, and is related to w and g through the following relation

$$N = 1/(w+g) \tag{22}$$

The capacitance C per unit length is given by

$$C = 2\pi\varepsilon_1/\ell n\left(\frac{a}{d}\right) \tag{23}$$

and the phase velocity, v, is given by

$$v = 1/(C\ Z_o) \tag{24}$$

Table 6 lists calculated values of Z_o and the normalized phase velocity v/v_o for the configuration of Figure 9. Note that the dielectric constant ε_2 does not enter into the expression for Z_o. Here, the specified values of N correspond to the following reasonable examples, in accordance with (22).

N = 125; w = 0.006"; G = 0.002"
N = 165; w = 0.006"; G = 0
N = 250; w = 0.002"; G = 0.002"

It is interesting to note, that the data in Table 6 indicates that Z_o approaches a limiting value as μ_{r2} increases indefinitely, this is because the inductance in the limit of high μ_{r2} is determined by the reluctance of the flux path presented by the region occupied by the MOV material. Note also that the values of Z_o in Table 6 for $\mu_{r1} = \mu_{r2} = 1$ are higher than the values given in Tables 3 and 4 for a microstrip configuration having corresponding values of w/h.

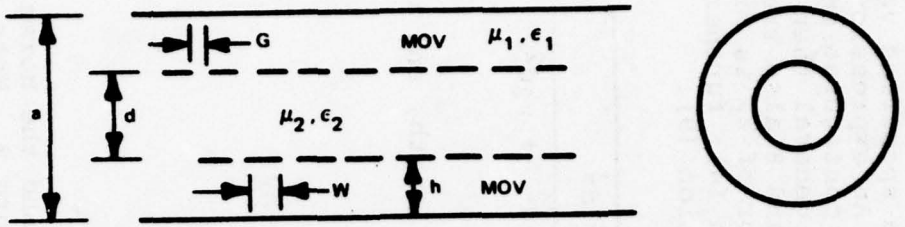


Figure 9. Coaxial Line with Helical Center Conductor.

TABLE 6. Characteristic Impedance and Normalized Phase Velocity for the Co-axial Line with a Helical Center Conductor. Shown in Figure 9

$a = 0.104$ inches

$d = 0.052$ inches

$\mu_{R1} = 1$

$\epsilon_{R1} = 1000$

N	μ_{R2}	Z_o (OHMS)	V/V_o
250	1	39.5	.001053
	3	55.8	.000744
	10	69.2	.000600
	30	75.3	.000552
	100	77.8	.000534
165	1	26.1	.001595
	3	36.8	.001128
	10	45.7	.000909
	30	49.7	.000836
	100	51.3	.000809
125	1	19.7	.002105
	3	27.9	.001488
	10	34.6	.001200
	30	37.6	.001104
	100	38.9	.001068

The higher values of Z_o for the configuration of Figure 9 result from the increased inductance per unit length due to mutual coupling between the turns provided by the helical center conductor. However, in spite of the increased inductance, Table 6 shows that with a non-magnetic core (i.e., $\mu_{r2} = 1.0$) one cannot obtain a value of 50 ohms for Z_o even with strip widths as small as w = 0.002".

With w = 0.006", G = 0 and w/h = 0.23, a value of 50 ohms is obtained for Z_o when μ_{r2} lies between 30 and 40. This value of w/h corresponds closely to the value of w/h which yielded Z_o = 50 ohms for the microstrip configuration of Figure 6.

It can be shown that for large values of μ_{r2} and for values of (a-d) << a, the characteristic impedance of the coaxial line with helical center conductor corresponds exactly to that of the microstrip configuration of Figure 6, provided also that G<< w. Under the above conditions, (21) reduces to

$$Z_o = \sqrt{\frac{\mu_1}{8\epsilon_1} N^2 \, (a^2-d^2) \, \ell n \, \frac{a}{d}} \qquad (25)$$

Since d = a - 2h,

$$a^2-d^2 = 4 \, a \, h \qquad (26)$$

Furthermore,

$$\ell n \left(\frac{a}{d}\right) = \ell n\left(\frac{a}{a-2h}\right) = \frac{2h}{a} \qquad (27)$$

Letting $N^2 = 1/w^2$ and substituting (26) and (27) into Equation (25) yields

$$Z_o = \frac{h}{w} \sqrt{\frac{\mu_1}{\epsilon_1}} \qquad (28)$$

which is identical to the value of Z_o given by (6) for the configuration of Figure 6.

The phase shift per turn for the configuration of Figure 9 can be calculated as was done for the case of the flat spiral of Figure 8. If $\mu_{r2} >> 1.0$, then (20) also applies for configuration of Figure 9 and the phase shift per unit length β is 37.9 degrees per cm at 100 MHz for $\epsilon_{r1} = 1000$, $\mu_{r1} = 1.0$. For the configuration of Figure 9, if a = 0.104", d = 0.052", h = 0.026", the length of one turn is equal to $\pi d = 0.4149$ cm. In this case, the phase shift per turn is 15.73 degrees. Note that this value is independent of the strip width, w, or MOV thickness, h, provided $\mu_{r2} >> 1.0$.

The total number of turns is equal to the total length of helical conductor divided by the length per turn, πd. As an example, let the total length be equal to 78.74 cm (as was calculated in Section 3.1.1 for a total conduction area of 1.0 square cm and a strip width of 0.005"). In this case, 190 turns are required. For a strip width w = 0.005", and gap, G = 0.002", the number of turns per inch is equal to 143. The total length of helix is, therefore, 1.330 inches.

3.1.4 Coaxial Line With Helical Center Conductor-Varistor Material in Angular Sector Less Than 360°

In order to obtain a wider strip width for a given Z_o, the MOV material can be confined within an angular sector θ which is less than 360° as shown in Figure 10. In this case, the inductance has the same value as for the configuration of Figure 9, while the capacitance is decreased by a factor approximately equal to $\theta/360$. This assumes that $\varepsilon_{r1} >> 1$ as is typically the case for MOV material. Under these conditions, the value of Z_o for the configuration of Figure 10 is given by

$$Z_o = \sqrt{\frac{360}{\theta} \quad \frac{\mu_1}{\varepsilon_1}} \; \frac{h}{w} \qquad (29)$$

where θ is in degrees. Thus, if $\theta = 90°$, the value of w for Z_o = 50 ohms is twice the value for $\theta = 360°$.

It follows that the insertion loss due to copper losses and MOV dielectric losses can be made smaller with this configuration. Furthermore, it may be possible to eliminate the need for a ferrite material by increasing the "can" diameter, a, and by placing the helix non-concentrically with respect to the can. In this way, the inductance per turn is increased by reducing the effect of the image current in the can over part of the length of the turn. It should be noted, however, that the configuration is a low pass structure with an upper cutoff frequency.

3.1.5 Transverse Laminations in Coaxial Lines

Figure 11 shows how MOV discs can be cascaded with high-permeability discs to obtain an effective characteristic impedance of, say, 50 ohms. This is actually a low pass filter structure with the MOV discs acting essentially as the shunt capacitors and the high-permeability discs acting essentially as series inductors. The equivalent circuit is shown in Figure 12. For the purpose of the present discussion, it will be assumed that the filter comprises a cascade of identical pairs of discs, except for the first and last MOV discs which have half thickness. This corresponds to a uniform-element filter. One could also consider a cascade of non-uniform discs in order to obtain somewhat more desirable transmission characteristics.

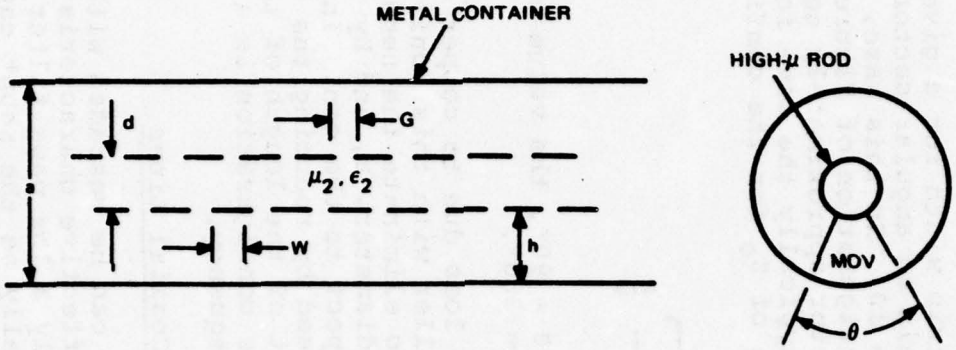


Figure 10. Coaxial Line with Helical Center Conductor (Metal Oxide Varistor Material in Angular Section <360°).

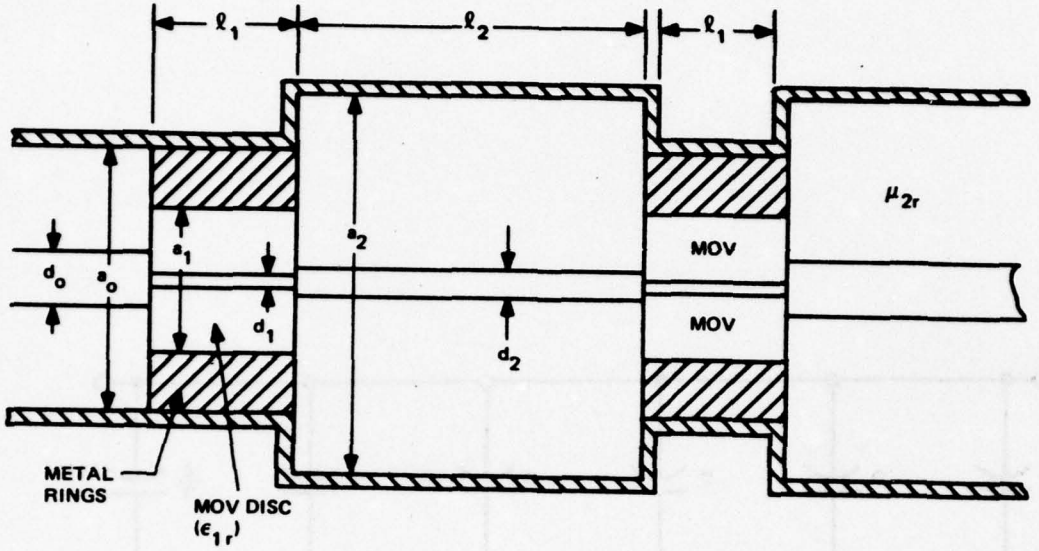


Figure 11. Metal Oxide Varistor and High-μ Discs Cascaded in a Coaxial Line.

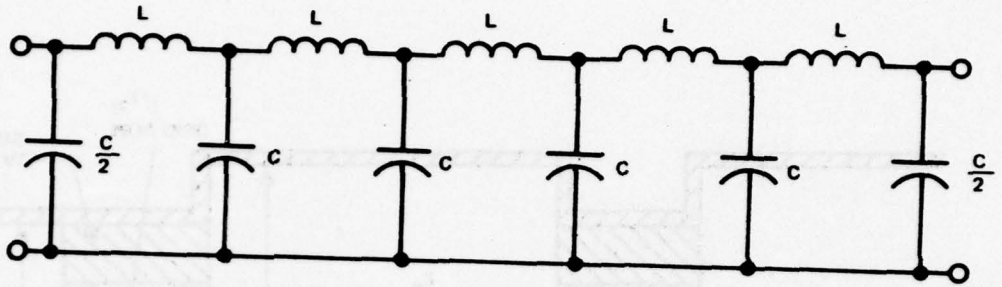


Figure 12. Equivalent Circuit for the Configuration Shown in Figure 11.

The transmission characteristics can be calculated by neglecting the inherent inductance of the MOV discs and the inherent capacitance of the high-permeability discs. The discontinuity capacitances have also been neglected. Under these approximations, the values for the elements of the equivalent circuit are given by

$$C = (2\pi\varepsilon_1 \ell_1)/\ell n \left(\frac{a_1}{d_1}\right) \tag{30}$$

$$L = \frac{\mu_2 \ell_2}{2\pi} \ell n \left(\frac{a_1}{d_2}\right) \tag{31}$$

The characteristic impedance, Z_o, is given by

$$Z_o = \sqrt{\frac{\mu_{2r}\ell_2}{\varepsilon_{1r}\ell_1}} \sqrt{Z_{10}Z_{20}} \tag{32}$$

where

$$Z_{no} = \frac{1}{2\pi} \sqrt{\frac{\mu_o}{\varepsilon_o}} \ell n \left(\frac{a_n}{d_n}\right) \tag{33}$$

is the characteristic impedance of the MOV ($n = 1$) region or the high-μ ($n = 2$) region when these regions have vacuum as the medium; ε_o and μ_o corresponds to the vacuum values in this case. The cutoff frequency, f_c, for the low pass filter is given by

$$f_c = \frac{1}{2\pi}\sqrt{\frac{4}{LC}} \tag{34}$$

$$f_c = \frac{v_o}{\pi} \sqrt{\frac{1}{\mu_{2r}\ell_2\varepsilon_{1r}\ell_1}} \sqrt{\frac{Z_{10}}{Z_{20}}} \tag{35}$$

where v_o is the free space velocity.

Equations (32) and (35) can be solved for ℓ_1 and ℓ_2 as a function of the specified values of Z_o, Z_{10}, Z_{20}, f_c, μ_{2r} and ε_{1r}. The results are

$$\ell_1 = \frac{v_o Z_{10}}{\pi f_c Z_o \varepsilon_{1r}} \tag{36}$$

$$\ell_2 = \frac{v_o \, z_o}{\pi \, f_c \, z_{20} \, \mu_{2r}} \qquad (37)$$

Equations (36) and (37) are the desired design equations. As a simple example, let $a_1 = a_2 = a_o$, the outer diameter of the input line and $d_1 = d_2 = d_o$, the center conductor of the input line. The following design values will also be assumed

$$\mu_{2r} = 20$$

$$\varepsilon_{1r} = 1000$$

$$v_o = 3 \times 10^{10} \text{ cm/sec}$$

In this case,

$$\ell_1 = 0.047 \text{ cm} = 0.0185"$$

$$\ell_2 = 2.387 \text{ cm} = 0.940"$$

The value of ℓ_1 may be a reasonably practical value, but ℓ_2 is too large since an impractically long device would be required to achieve a large value of conduction area for the MOV material. The following additional calculations bear this out. In this first example, a value of 50 ohms has been assumed for Z_{10} and Z_{20}. If it is also assumed that $(a_1-d_1)/2 = 0.065$ cm in order to obtain a clamping voltage of 100 volts, d_1 is equal to 0.040" and a_1 is equal to 0.092". In this case, the conduction area of each MOV disc is equal to 0.0015 square cm. The number of discs for 1 square cm area is, therefore, 67. With the above values of ℓ_1 and ℓ_2, the total device length is equal to 63.9 inches.

3.1.6 Ridge Waveguide High Pass Filter

The ridge waveguide configuration shown in Figure 13 is a purely distributed parameter configuration. Since it has a low-frequency cutoff for transmission, this configuration represents a high pass filter approach. As will be shown below, this configuration actually has little promise, and a discussion of its characteristics has been included in this report only as an example of this class of waveguide configuration.

The cutoff frequency can be determined from the condition

$$\frac{\omega_c C}{2} = \frac{1}{\eta b \tan \theta_c} \qquad (38)$$

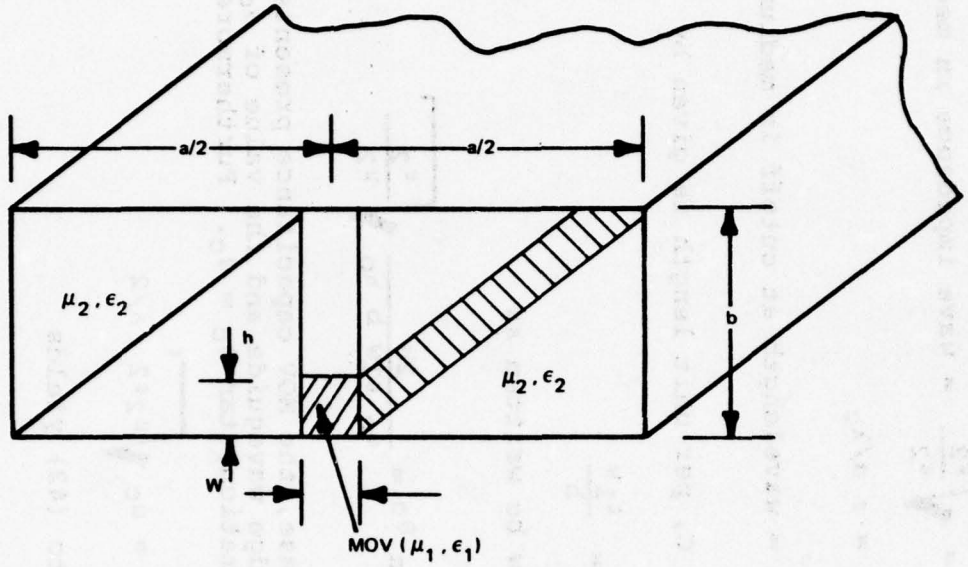


Figure 13. Metal Oxide Varistor in Ridge Waveguide Configuration.

where

$$\begin{cases} \omega_c = 2\pi f_c & (39) \\ C = \text{MOV capacitance per unit length} \\ \eta = \sqrt{\dfrac{\mu_2}{\varepsilon_2}} = \text{wave impedance in medium 2} \end{cases}$$

$$\begin{cases} \theta_c = \pi\, a/\lambda_c & (40) \\ \lambda_c = \text{wavelength at cutoff in medium 2} \end{cases}$$

The MOV capacitance, C, per unit length is given by

$$C = \frac{\varepsilon_1 w}{h} \tag{41}$$

Equation (38) can now be written as

$$\tan \theta_c = \frac{2h}{\omega_c\, \varepsilon_1 w\, b\, \eta_o} \sqrt{\frac{\varepsilon_2}{\mu_2}} \tag{42}$$

In the present case, the MOV capacitance presents a high degree of loading on the ridge waveguide and the value of θ_c is small, allowing the approximation, $\tan \theta_c = \theta_c$. Furthermore,

$$\theta_c = \omega_c \sqrt{\mu_2 \varepsilon_2}\ \ a/2 \tag{43}$$

Substituting (43) into (42) yields

$$ab = \frac{4h}{\omega^2_c\, \mu_2 \varepsilon_1 w} \tag{44}$$

Note that ε_2 has dropped out of the analysis. Note also that the cross sectional area, ab, is inversely proportional to μ_2.

The following are considered practical values for the variables in (44).

$$h = 0.026" \text{ (for 100 volt device)}$$

$$w = 0.030"$$

$$\varepsilon_1 = 1000 \times 8.854 \times 10^{-12} \text{ Farads/meter}$$

$$\mu = 20 \times 4\pi \times 10^{-7} \text{ Henries/meter}$$

Substitution of these values in (44) results in

$$ab = 39.46 \text{ square cm}$$

For a square cross section

$$a = b = 6.282 \text{ cm} = 2.473"$$

The total length is 13.123 cm = 5.167".

From the point of view of the cross sectional dimensions and length, it appears that the above configuration is practical. However, the transmission characteristics have not been analyzed in detail. It is known that at the cutoff frequency, the MOV capacitance is tuned by the inductance of the waveguide. The length of ridge waveguide is, therefore, essentially a parallel tuned capacitor and inductor. If the input and output lines have 50 ohms impedance, the loaded Q is given by

$$Q = 25\omega_c C \tag{45}$$

$$Q = \frac{25\omega_c \varepsilon_1 w}{h} \tag{46}$$

Substituting the above values, there results Q = 2.105 at 10 MHz. Since $Q = \omega_c/\Delta\omega$, the bandwidth $\Delta f = \Delta\omega/2\pi$ between 3 dB points is given by

$$\Delta f = h/(50\pi\ \varepsilon_1 w\ell) \tag{47}$$

Thus, the absolute bandwidth is independent of the cutoff frequency. For the above values, Δf = 4.74 MHz. About 20 units would be needed to cover the range between 10 and 100 MHz with 3 dB insertion loss at the edges of each band.

3.1.7 Distributed Parameter Analysis Summary

Calculations have shown that the strip widths required for 50-ohms characteristic impedance for the conventional microstrip configuration of Figure 4 are impractically small. An analysis of the modified microstrip configuration of Figure 6 employing ferrite material was performed. The results indicate that a strip width of 0.005" is required for a 50-ohms line having a clamping voltage of 100 volts. It was established that $\mu \sim 16$ is required. Calculation of the attenuation (conductor, ferrite and dielectric losses) shows that dielectric losses predominate.

The following examples show what can be achieved with the microstrip configuration as a function of conduction area and clamping voltage if a total of 1.0 dB maximum insertion loss is specified. In both cases the length of the microstrip line is 10.68 cm.

a. Clamping volts = 100	b. Clamping volts = 737
h = 0.026"	h = 0.192"
w = 0.005"	w = 0.037"
ℓ = 10.68 cm	ℓ = 10.68 cm
A = 0.1357 sq cm	A = 1.0 sq cm

The analysis has also shown that all of the "purely distributed" configurations that have been studied suffer from the same problems as the microstrip configuration. These configurations can not result in significantly lower loss than the microstrip configuration, and have the added disadvantage of fabrication difficulty.

The coaxial configuration of Figure 10, which is actually a lumped-element configuration, can have lower losses than the microstrip configuration. However, this too has fabrication problems, and is probably not an optimum lumped-element configuration from the point of view of losses or ease of fabrication.

3.2 Lumped Parameter Configuration

As was the case with the distributed parameter approach, the principle design problem to be addressed in integrating the metal oxide varistor into a lumped parameter configuration is also associated with the high value permitivity of the material. The principle design technique used in the distributed paramater configuration was to approach this problem from a geometrical standpoint in an effort to define the optimum transmission line geometry to meet the insertion loss requirements. The principle design technique for the lumped parameter approach, on the other hand, was to treat the varistor as a discrete circuit element and evaluate various methods to tune out its capacitive reactance. As such, the main design efforts were centered on evaluating various tuned circuit and filter configurations in order to define the optimum circuit which would maximize

the amount of varistor material capable of being integrated into a terminal protection device.

A variety of circuit configurations were considered during the study. These included single and multi stage lowpass and bandpass filters of the Butterworth, Chebyshev, Elliptic, Bessel, Image Parameter and Cascaded Parallel Resonance type as well as the Constant-K in a complexity of stages for various ripple factors. The filters were evaluated parametrically in terms of total MOV area to thickness ratios such that by defining the desired clamping voltage (related to thickness) and desired energy capability (related to area) one can choose the filter types and complexity order to achieve minimum insertion loss.

The design analyses associated with these studies are discussed in the following subsections.

3.2.1 Configuration Evaluation

In treating the varistor as a discrete circuit element, one can consider it to behave essentially as a medium Q capacitor in the unenergized state. The medium Q capacitor, in turn, can be modeled as a paralled plate type capacitor (neglecting fringing effects) with a parallel loss resistance across it. Then, in terms of the varistor area, A, and thickness, x, the varistor capacitance, C, parallel loss resistance, R_p, and quality factor, Q, is given by

$$C = \frac{\varepsilon_R \varepsilon_o A}{X} \tag{48}$$

$$R_p = \frac{\rho X}{A} \tag{49}$$

$$Q = 2\pi f C R_p = 2\pi f \varepsilon_R \varepsilon_o \rho \tag{50}$$

where

ε_o = permitivity of free space = 8.854×10^{-14} farads/centimeter

ε_R = relative dielectric constant of the varistor (see Figure 2)

ρ = parallel resistivity of the varistor (See Figure 2)

f = operating frequency in Hertz

C, R_p and Q can then be evaluated directly from the data given in

Figure 2. Figure 14 shows the typical values associated with the type DD varistor material at a 100 MHz operating frequency.

From a circuit element characterization such as this, it becomes a relatively straightforward task to define varistor loss effects and to evaluate various lumped circuit configurations for compensation. Figure 15, for example, shows the voltage insertion loss effects as a function of varistor area to thickness ratio for the type DD material in a 50 ohm system. The associated phase distortion effects are shown in Figure 16. Thus, to achieve the desired insertion loss levels in a lumped parameter configuration requires one to provide an adequate compensation network to "detune" these effects.

There is, however, a finite extent to which this compensation can be achieved, being limited by the dissipative losses associated with the varistor resistance. The insertion loss effects associated with just this aspect of the varistor material is shown in Figure 17. These characteristics then define the maximum extent to which compensation can be accomplished if one achieved 100% capacitive compensation efficiency and were just left with the resistive losses of the material to contend with. Thus, to approach this limit was the goal of the present study.

The simplest form of compensation network, although admittedly not very broad band, would be a parallel resonance tuned circuit where the capacitor is formed by the varistor. Then, appropriate bandpass filters to cover discrete bandwidths of interest can be defined. One such group of bands in the present study was the 3 to 30 Megahertz band and the 30 to 70 Megahertz band. Figure 18 shows the voltage insertion loss effects incurred with employing the varistor in a single parallel resonant circuit tuned to cover the 3 to 30 Megahertz band. The associated voltage phase shift is shown in Figure 19. The dependence of the required tuning inductor size on varistor geometry is shown in Figure 20. Figures 21 and 22 show the voltage insertion loss and phase shift for the 30 to 70 Megahertz band. It can be seen that in both cases large insertion loss and phase shift is incurred off center frequency for any reasonable size varistor area to thickness ratio. Hence, it is rather obvious from these results that somewhat more sophisticated filter configurations are required.

In going to a more sophisticated filter configuration one can choose from a variety of established filter types such as Butterworth, Chebyshev, Elliptic, Bessel, Image Parameter, Constant-K, etc. Furthermore, one can select from a variety of ripple factors and number of stages to tailor the filter configuration to a particular requirement. Each of the various filters types offer to optimize one particular characteristic parameter at the expense of the remaining ones. One can select, for instance, a filter which will offer maximally flat response over a certain band, one with minimum or maximum linear phase shift, one with maximum bandwidth for losses below particular levels, etc.

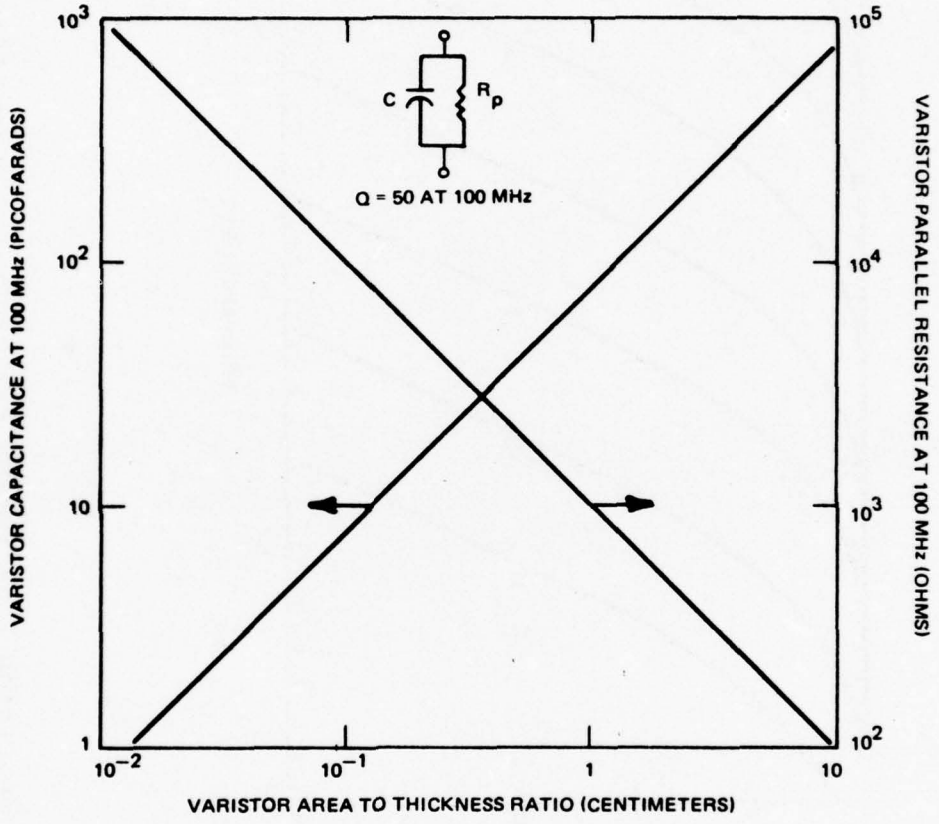


Figure 14. Capacitance and Loss Characteristics of the Type DD GE-MOV^R Varistor Versus Varistor Area to Thickness Values.

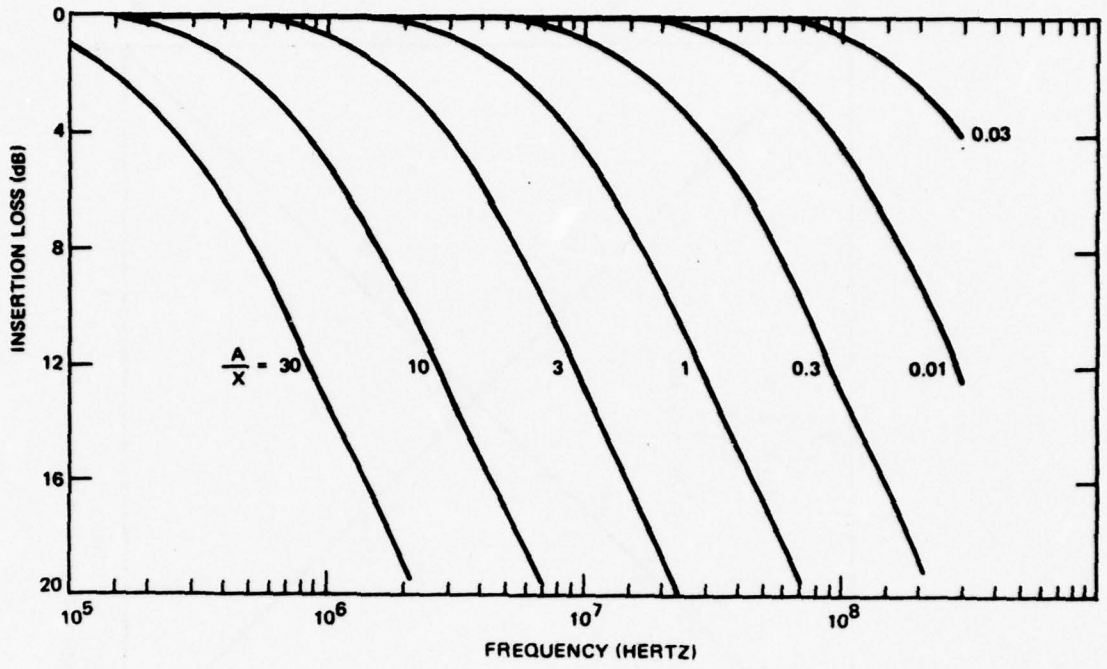


Figure 15. Insertion Loss Versus Frequency Characteristics for Various Metal Oxide Varistor Area to Thickness Values.

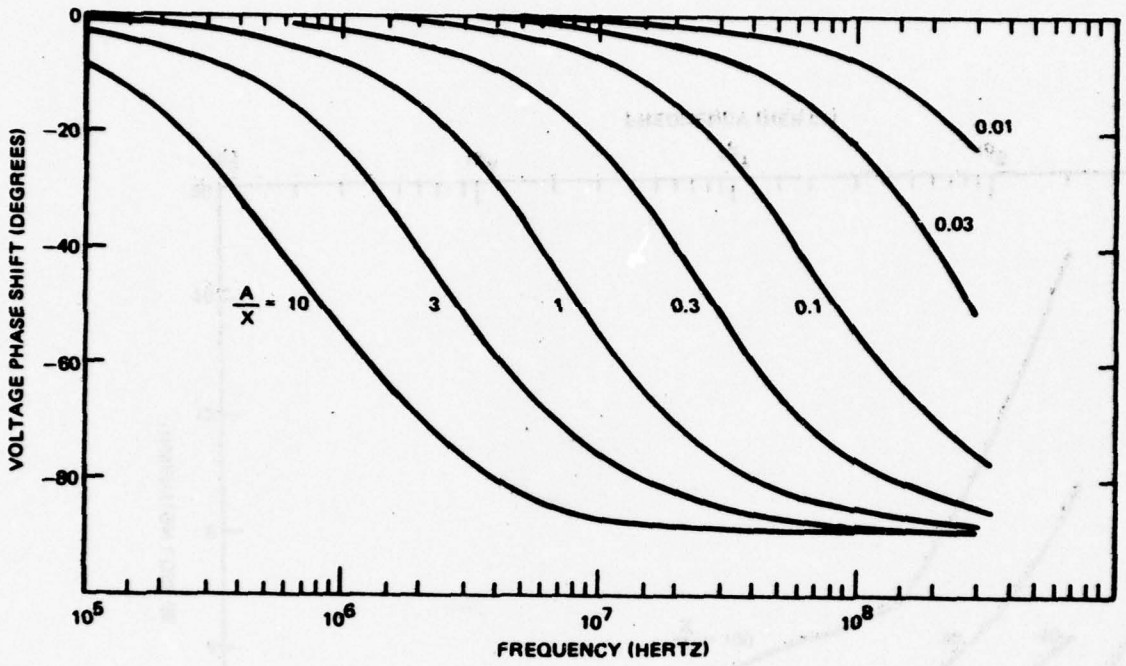


Figure 16. Phase Shift Versus Frequency Characteristics for Various Metal Oxide Varistor Area to Thickness Values.

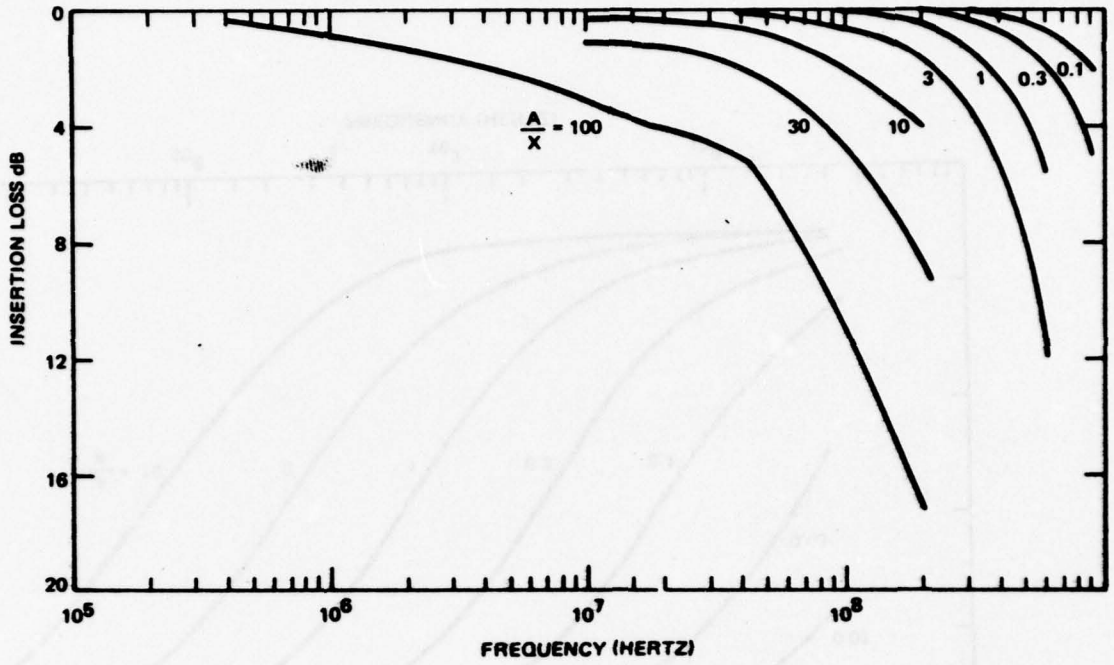


Figure 17. Insertion Loss Due to Dielectric Resistivity Versus Frequency for Various Metal Oxide Varistor Area to Thickness Values.

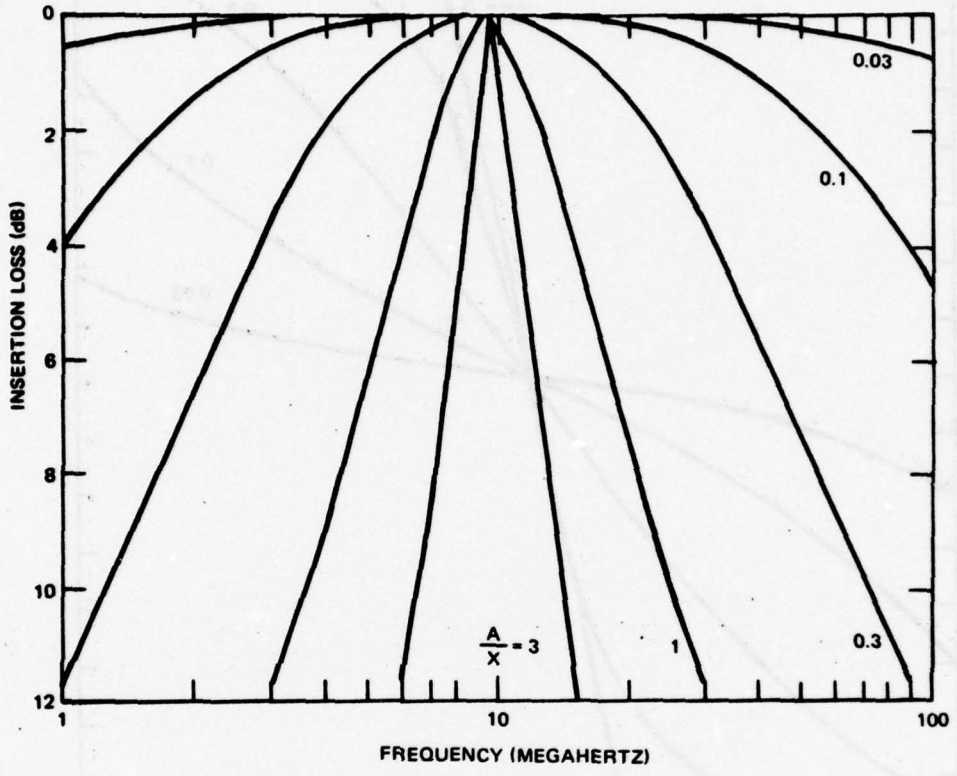


Figure 18. Insertion Loss Characteristics of a Single Stage Metal Oxide Varistor-Parallel Tuned Circuit for the 3 to 30 Megahertz Band.

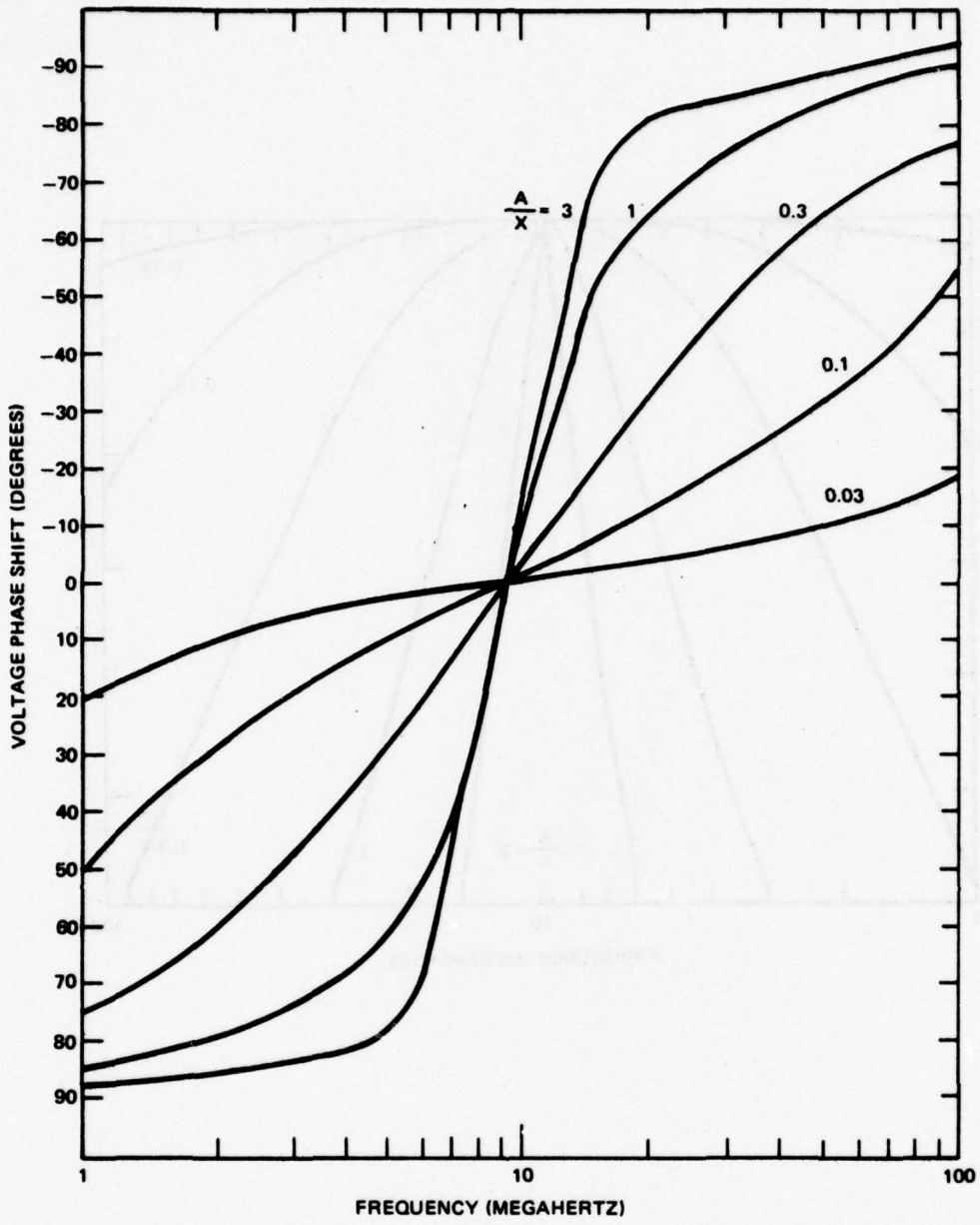


Figure 19. Phase Shift Characteristics of a Single Stage Metal Oxide Varistor-Parallel Tuned Circuit for the 3 to 30 Megahertz Band.

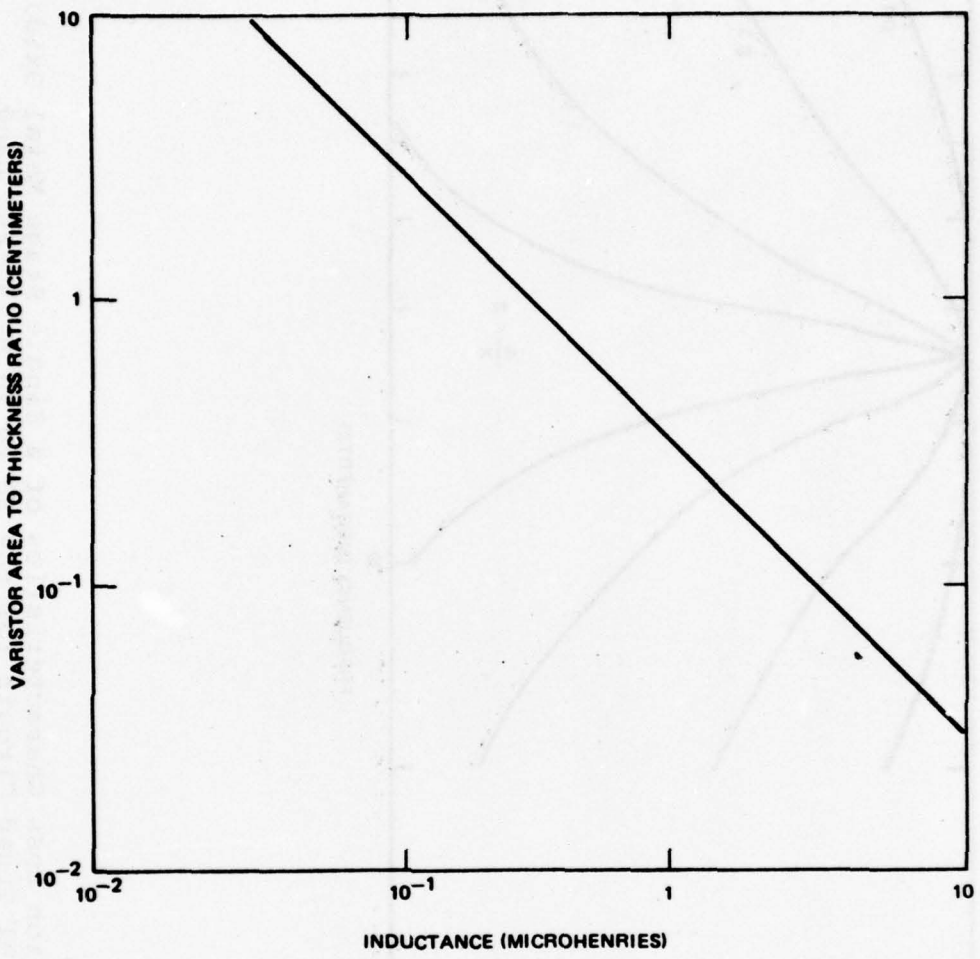


Figure 20. Inductance Requirements for a 3 to 30 Megahertz Band, Single Stage Metal Oxide Varistor-Parallel Tuned Circuit.

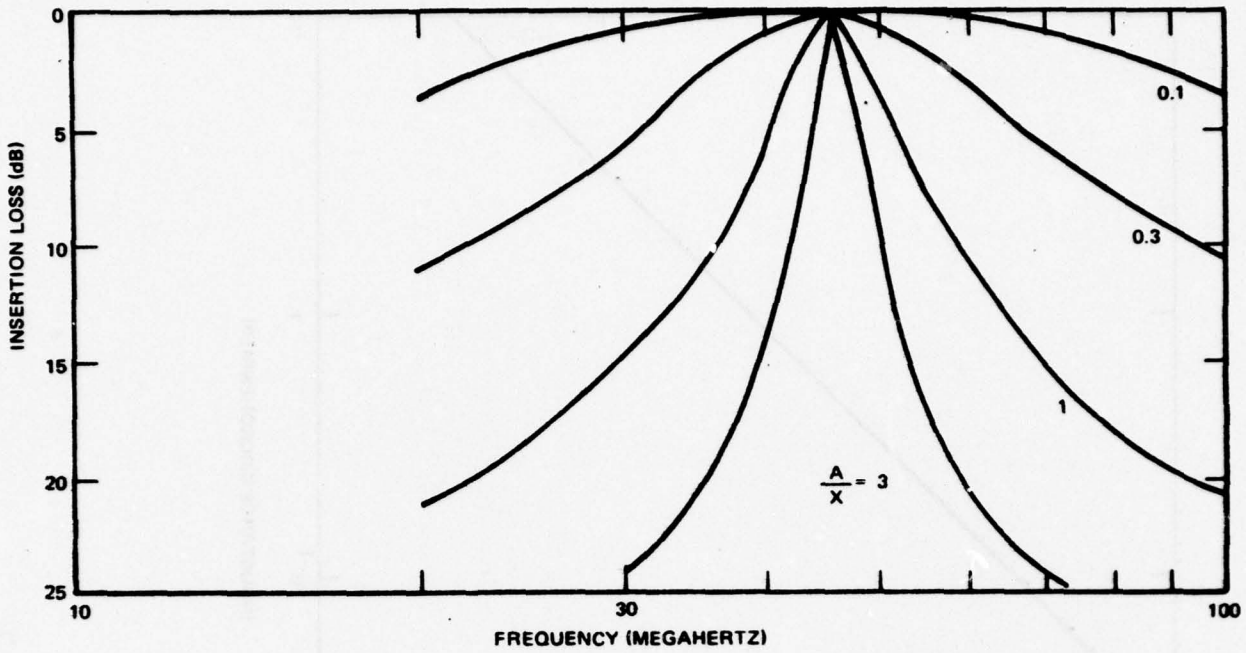


Figure 21. Insertion Loss Characteristics of a Single Stage Metal Oxide Varistor Parallel Tuned Circuit for the 30 to 70 Megahertz Band.

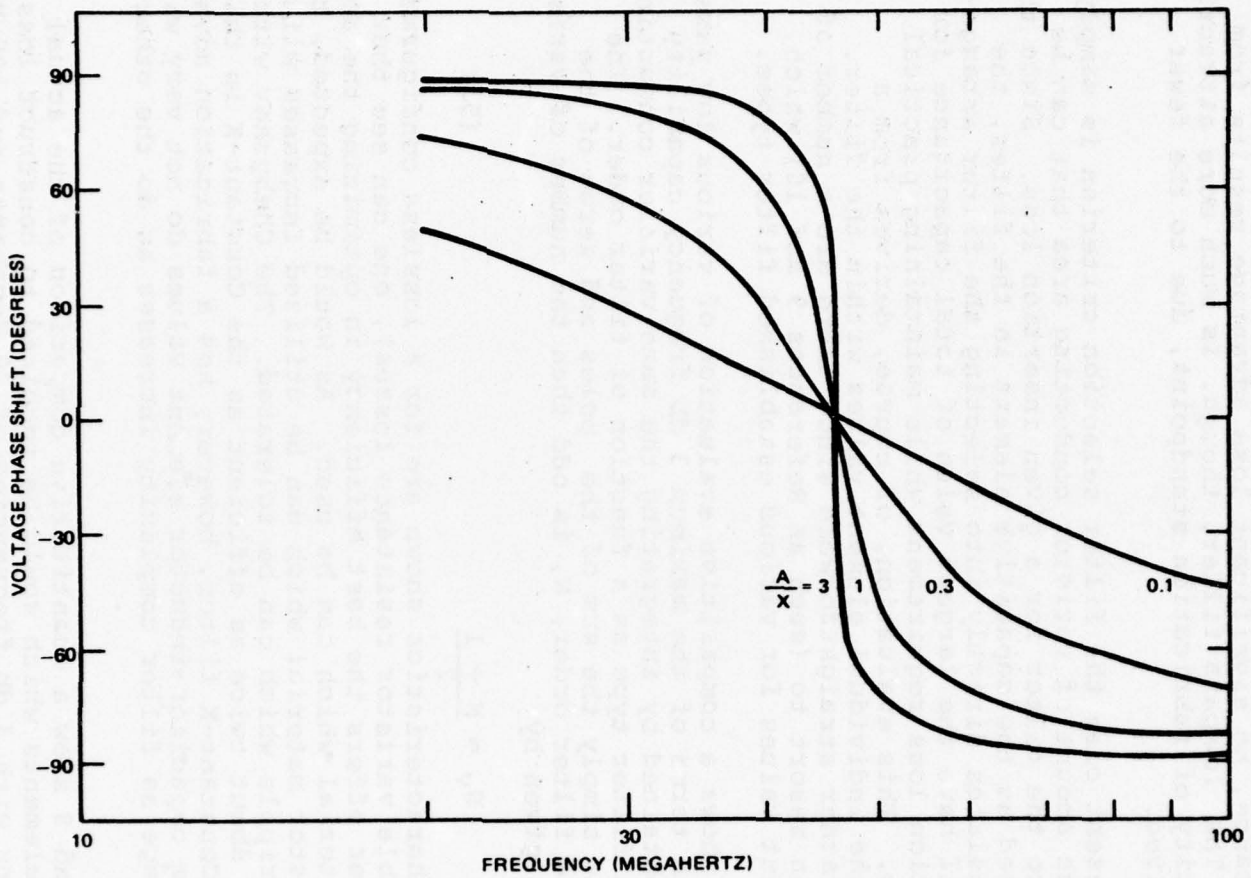


Figure 22. Phase Shift Characteristics of a Single Stage Metal Oxide Varistor-Parallel Tuned Circuit for the 30 to 70 Megahertz Band.

One further variation in filter configuration that one can consider is the choice between a bandpass or low pass type. However, since the upper cutoff frequency of a bandpass filter and the cutoff frequency of a lowpass filter are determined by the filter capacitance, no significant loss advantage results from either type. The lowpass filter, though, is much more attractive from a simplicity of fabrication standpoint, due to the fewer elements involved.

In the present case the filter selection criterion is simply to maximize the amount of varistor conducting area that can be integrated into the filter for a given insertion loss. Since the varistor is used as the capacitive element in the filter, the criterion translates directly into selecting the filter arrangement which will have the largest value of total capacitance for a given insertion loss requirement while maintaining practical element values. This evaluation, of course, derives from a knowledge of the individual element values within the filter. This task is rather straightforward since there are a number of sources one can resort to (such as References 9 and 10) which tabulate element values for various established filter types.

Figure 23 shows a comparitive evaluation of various low pass filter types in terms of the maximum 3 db frequency capability which can be obtained by integrating the same varistor conducting area into each filter type as a function of filter order. The filter order is simply the sum of the poles and zeros of the filter. If the filter order, N, is odd than the number of varistor elements N_v is given by

$$N_v = \frac{N + 1}{2} \qquad (51)$$

Although the characteristics shown are for a lossless configuration (i.e., negligible varistor resistance losses), one can see that the Chebyshev filter offers the best efficiency in optimizing the amount of varistor material which can be used. As would be expected, the amount of varistor material which can be utilized increases with the amount of ripple which can be tolerated. The Chebyshev with 1 db ripple is about twice as efficient as the Constant-K in this respect. The Constant-K filter, however, has a fabrication advantage in that the capacitor-inductor element values do not vary within each filter stage as filter complexity increases as do the other types.

Tables 7 and 8 show a quantitative comparison of the actual values of the filter elements which would be required to construct lossless low pass filters with 3 db frequencies of 30 Megahertz and 100 Megahertz respectively. As shown, the various filters can be constructed using physically realistic element values, although the inductor values for the lower cutoff frequencies do start to approach large values.

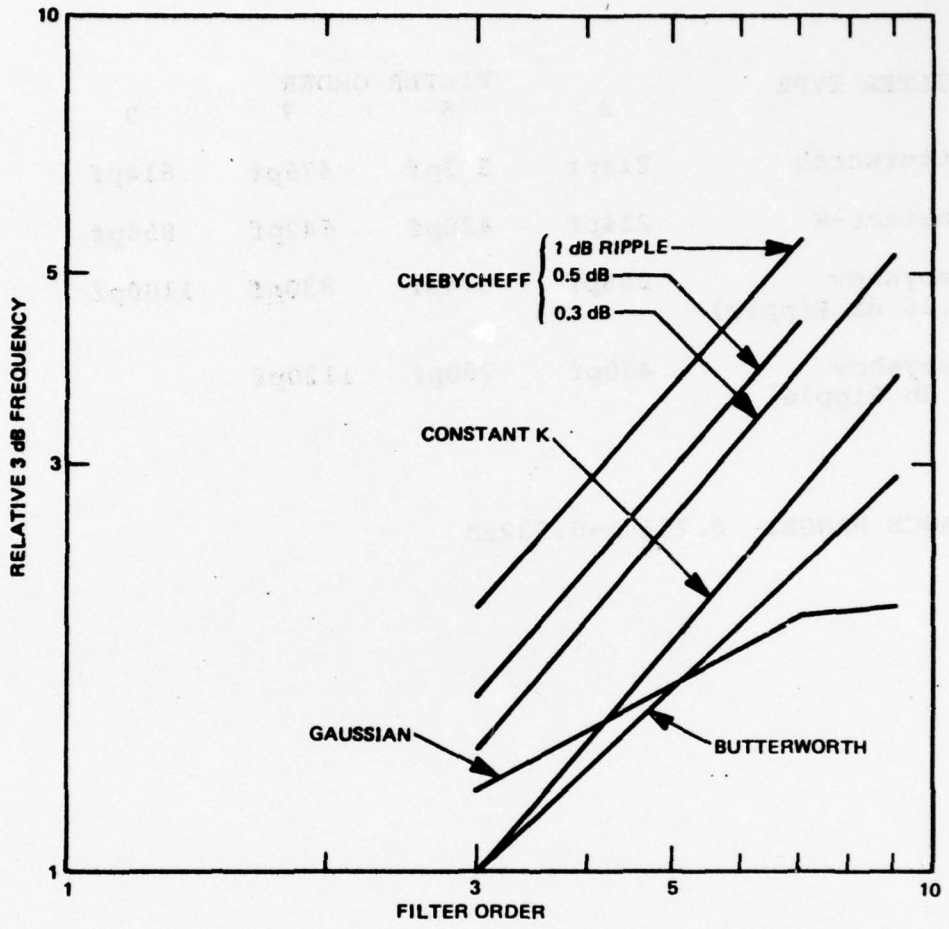


Figure 23. Comparison of Lossless Low Pass Filter Types for the Same Total Varistor Capacitance.

TABLE 7. Total Capacitance and Element Inductance for Various Lossless Low Pass Filter Types With a 30 Megahertz 3 db Frequency.

FILTER TYPE	FILTER ORDER 3	5	7	9
Butterworth	214pf	343pf	476pf	614pf
Constant-K	214pf	428pf	642pf	856pf
Chebyshev (0.28 db Ripple)	288pf	544pf	830pf	1100pf
Chebyshev (1 db Ripple)	430pf	780pf	1120pf	

INDUCTANCE RANGE: 0.266μh→0.532μh

TABLE 8. Total Capacitance and Element Inductance Values for Various Lossless Low Pass Filter Types With a 100 Megahertz 3 db Frequency.

FILTER TYPE	FILTER ORDER 3	5	7	9
Butterworth	64pf 0.16μh	103pf 0.13μh	143pf 0.10μh 0.16μh	184pf 0.08μh 0.15μh
Constant-K	64pf 0.16μh	128pf 0.16μh	192pf 0.16μh	256pf 0.16μh
Chebyshev (0.28 db Ripple)	86pf 0.09μh	163pf 0.11μh	248pf 0.11μh 0.12μh	330pf 0.12μh 0.15μh
Chebyshev (1 db Ripple)	129pf 0.08μh	233pf 0.09μh	335pf 0.09μh 0.10μh	

3.2.2 Constant-K Filter With Microstrip Inductors

As indicated in the previous section, the Chebyshev filter was found to be the most efficient configuration of the various types evaluated with respect to varistor material utilization. The Constant-K filter, however, is extremely attractive from its simplicity of fabrication standpoint and is 50% as efficient as the Chebyshev with 1 db ripple. Furthermore, any insertion loss characteristics which are shown feasible in a Constant-K configuration can be improved on by going to a more complex multistage Chebyshev configuration. It is for this reason, that the Constant-K filter was selected as the baseline for detailed evaluation as the candidate for the lumped parameter, terminal protection device configuration. A further simplification was to utilize microstrip inductors for the inductive filter elements, thereby negating any saturation and loss effects associated with ferrite coupled elements and parasitic capacitance effects of coils.

The Constant-K filter consists of a network of symmetrical cascaded "T" or "π" sections. The schematic representation of a "π" section is shown in Figure 24. The section consists of a total stage capacitance C_S and associated resistive loss R_{PS}, together with a stage inductance L_S and its associated resistive loss R_{SS}. For a lossless case (i.e., $R_{PS} = \infty$ and $R_{SS} = 0$), the filter possesses a certain characteristic impedance (often termed the iterative impedance), Z_O, which is purely resistive in the passband and phase change β per section which are both dependent on angular frequency and are given by (Reference 11).

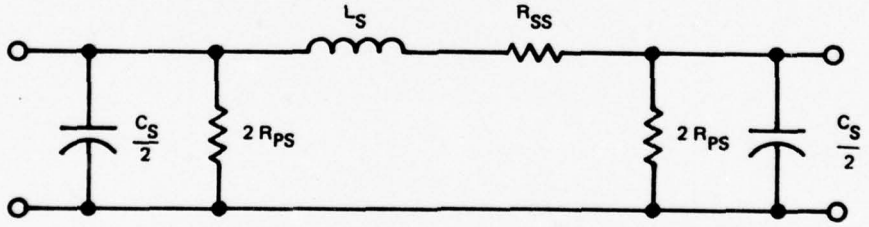


Figure 24. Single π Section of a Lossy Constant-K Filter

$$Z_o = \sqrt{\frac{L_s}{C_s \left[1 - \left(\frac{\omega}{\omega_c}\right)^2\right]}} \tag{52}$$

$$\cos \beta = 1 - 2 \left(\frac{\omega}{\omega_c}\right)^2 \tag{53}$$

$$\omega_c = 2\pi f_c = \frac{2}{\sqrt{L_s C_s}} \tag{54}$$

For $\omega < \omega_c$

$$Z_o \sim \sqrt{\frac{L_s}{C_s}} \tag{55}$$

and

$$C_s = \frac{2}{\omega_c Z_o} \tag{56}$$

$$L_s = (Z_o)^2 C_s = \frac{2 Z_o}{\omega_c} \tag{57}$$

Since the varistor material is used to form the filter capacitance, one can define the allowable varistor area, A_s, to thickness, X_s, ratio per section in terms of the characteristic impedance, Z_o, and cutoff frequency, f_c, by equating (48) and (56).

$$\frac{A_s}{X_s} = \frac{1}{\pi f_c Z_o \varepsilon_r \varepsilon_o} \tag{58}$$

The inductance per stage can similarly be defined by equating (48) and (57)

$$L_s = (Z_o)^2 \varepsilon_r \varepsilon_o \frac{A_s}{X_s} \tag{59}$$

The resistive losses of the capacitor elements are described in terms of the varistor, Q, and operating frequency, f, in (50)

$$Q_c = 2 \pi f C_s R_{ps} \qquad (50)$$

$$= 2 \pi f \varepsilon_r \varepsilon_o \rho$$

and are independent of varistor geometry. The resistive losses of the inductor elements are similarly described by

$$Q_L = \frac{2 \pi f L_s}{R_{ss}} \qquad (60)$$

where R_{ss} depends on the particular inductor type used.

Although the use of microstrip inductors, instead of ferrite or air coupled coils, is a less efficient approach with respect to total inductor length, it is an attractive configuration from a fabrication standpoint and is directly compatible with existing microwave techniques (see for example, References 11, 12, 13 & 14). In applying microstrip inductors one can resort to square or round spiral configurations to increase packing density and inductive coupling. The equations describing these configurations are known and can be found in a number of sources such as References 15, 16, 17, 18 & 19. In the spiral configuration, however, one is confronted with crossovers and must resort to multi-layer hybrid approaches. For this reason, the rectangular strip, which is the simplest form of microstrip inductor, was utilized to form the inductive filter element.

Terman (Reference 20) gives the low frequency inductance of a straight, rectangular strip of metal of length, ℓ, width, ω, and height, h, as

$$L = 5.08 \times 10^{-9} \ell \left\{ \ln \left(\frac{\ell}{\omega + h} \right) + 1.193 + 0.2235 \frac{\omega + h}{\ell} \right\} \qquad (61)$$

where L is in henries and all dimensions are in inches. The inductance values at high frequencies are affected by skin effect but are lower than those given by the low frequency formula by less than 6 percent (reference 21). For a copper inductor, the Q is given by (Reference 21)

$$Q = 4.81 \times 10^7 \sqrt{f}\,\frac{L}{K}\left(\frac{\omega+h}{\ell}\right) \qquad (62)$$

where K is a correction factor to account for current crowding from the corner of the ribbon and for $\omega/h > 4$ is given by (Reference 20)

$$K = 0.5 \log_{10}\left(\frac{\omega}{h}\right) + 1.05 \qquad (63)$$

Figure 25 shows the values of inductance and Q which can be obtained using 1 mil thick copper microstrip inductors as a function of inductor length. As shown, inductors with Q greater than 100 at 100 MHz are readily obtainable for realistic inductor sizes. It should also be noted that the varistor, Q, is 50 at 100 MHz. As such, one would expect the filter losses to be primarily due to the varistor losses.

A characteristic of the Constant-K filter is that if one or more sections are terminated by a resistance, Z_o, equal to the characteristic impedance no reflection occurs and the input impedance is equal to the characteristic impedance, as in the case of a transmission line. At frequencies above the cut-off, f_c, no propagation occurs; signals are strongly reflected at the input end and are attenuated rapidly down the line. Giacoletto (Reference 22), however, has analytically defined what the optimum termination resistance, r, should be for single section, lossless Constant-K filters in order for the input impedance to be as uniformly resistive as possible, for minimum reactive impedance and for the phase shift to be as linear as possible. For π sections, his results are $r = 1.5\ Z_o$ for uniform input resistance, $r = 2.06$ for minimum reactive impedance and $r = 1.65$ for maximum linear phase shift. The optimum value is defined as that which gives a minimum value, over the whole pass band, to the squares of the deviations from the desired condition.

The implication of this can be observed from the characteristics given in Figures 26 and 27. Shown here is the relative output power and input impedance response of a single section, lossless Constant-K filter when terminated in its characteristic impedance, Z_o, and when terminated in Giacoletto's optimum resistance of $r = 1.5\ Z_o$. Note from Figure 26, that although the properly terminated network exhibits maximally flat power transfer characteristics, the mismatched network provides increased bandwidth for insertion losses less than 1 db. The impact of this with respect to the varistor can be understood by examining (58) and recalling that the termination impedance, r, is actually the

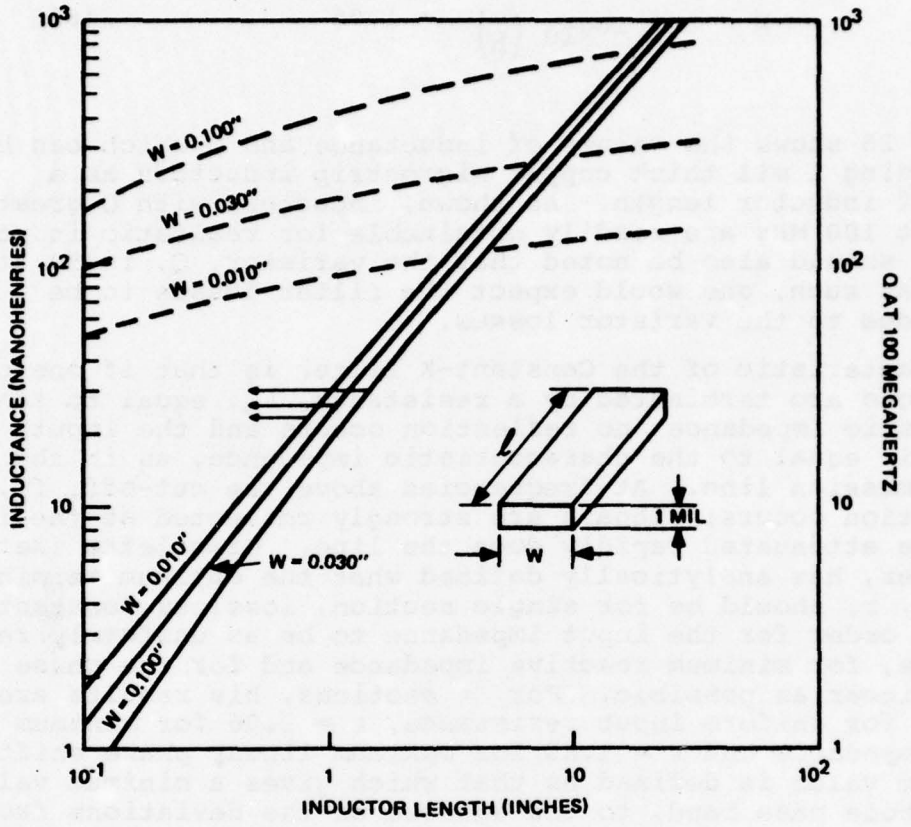


Figure 25. Inductance and 100 Megahertz Q Values for Flat Ribbon Wire.

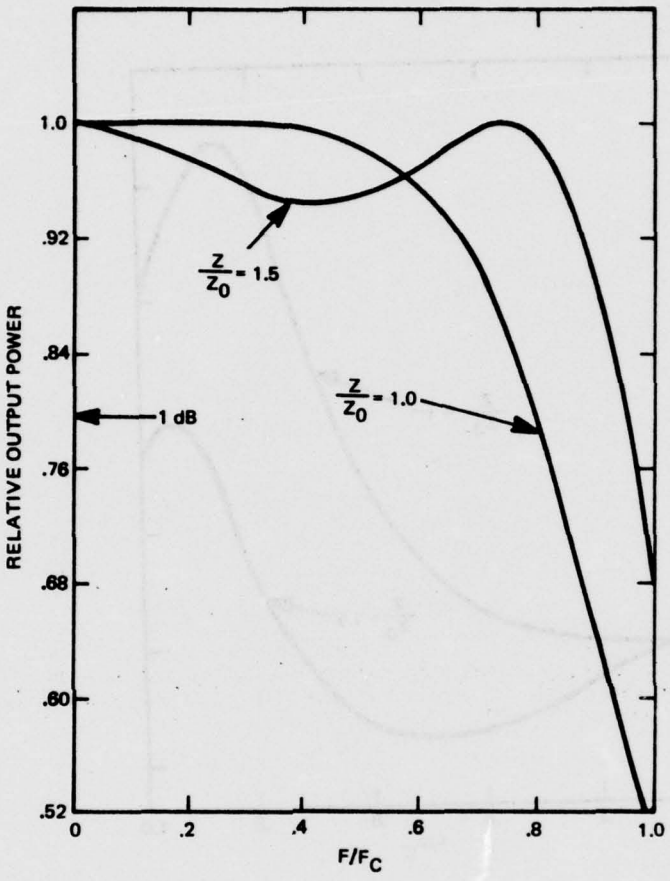


Figure 26. Output Power Characteristics of a Matched and Unmatched Optimally Terminated, Single Section, Lossless Constant-K Filter.

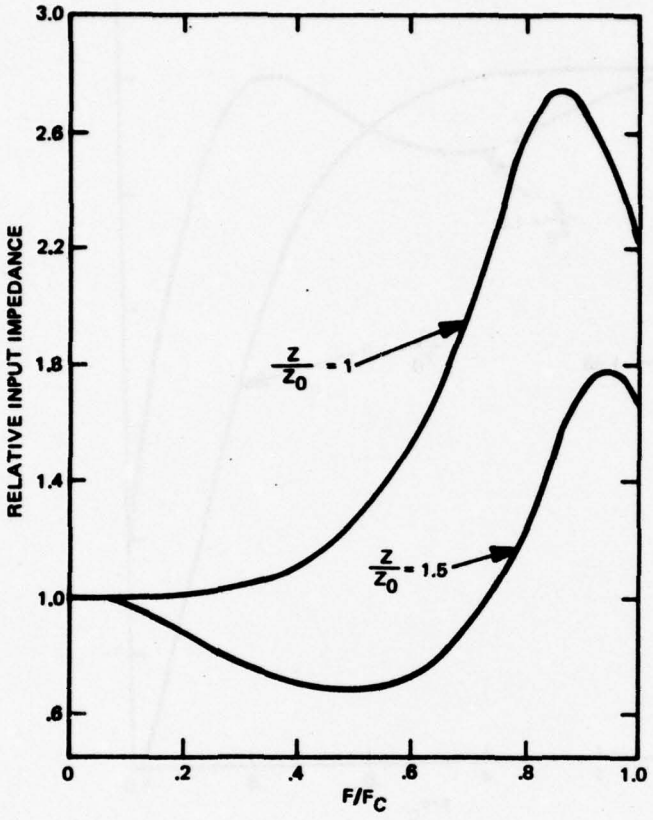


Figure 27. Input Impedance Characteristics of a Matched and Unmatched Optimally Terminated, Single Section, Lossless Constant-K Filter.

impedance of the network in which the varistor filter will be inserted. Hence, according to Giacoletto's results, the characteristic impedance should be less than r for optimum power transfer. Since the varistor area to length ratio is inversely proportional to Z_o, one should use more varistor material for optimum power transfer than would be required for a matched filter.

Giacoletto's equations, unfortunately, are only for a single section, lossless configuration. Furthermore, the set of equations defining this simple situation are, to say the least, unwieldy. In our present study, we are faced with describing a multisection, lossy filter and are faced with optimizing the number of stages and how close to cutoff one should design the filter to. Here, the analytical expressions describing this situation would become completely intractable. As such, recourse was made to computerized solutions employing multiple regression analyses to define a simplified best fit expression for a generalized lossy filter arrangement. Solutions were performed for 1 to 50 stage Constant-K filters employing varistors as the capacitive elements and for various inductor Q's. The results were a suprisingly simplified expression describing insertion loss in terms of the operating frequency, f/f_c, and number of stages, N. For a lossless inductor, the insertion loss for a matched filter ($r = Z_o$) is

$$db = 0.213\ (f/f_c)N \tag{64}$$

and for a matched filter employing inductors with a worst case Q of 100 at 100 MHz

$$db = 0.315\ (f/f_c)N \tag{65}$$

Similar solutions were performed for numerous conditions of mismatch (i.e., $r \neq Z_o$). The results of these analyses are shown in Figure 28 for an inductor Q of 100 at f_c and in terms of the quantity, $NfZ/f_c\ Z_o$, which will be shown to be related to total varistor area to length ratio which can be integrated into the filter. As such, Figure 28 defines the optimum filter characteristic impedance which will maximize the amount of varistor material in the filter for various allowable insertion losses.

From (58) the allowable varistor area to length ratio, A_s/X_s is given by

$$\frac{A_s}{X_s} = \frac{1}{\pi f_c\ Z_o\ \varepsilon_r\ \varepsilon_o} \tag{58}$$

The total amount of varistor material in the filter, A_T/X, is is simply the number of stages, N, times (58) or

$$\frac{A_T}{X_s} = \frac{N}{\pi\ f_c\ Z_o\ \varepsilon_r\ \varepsilon_r} \tag{66}$$

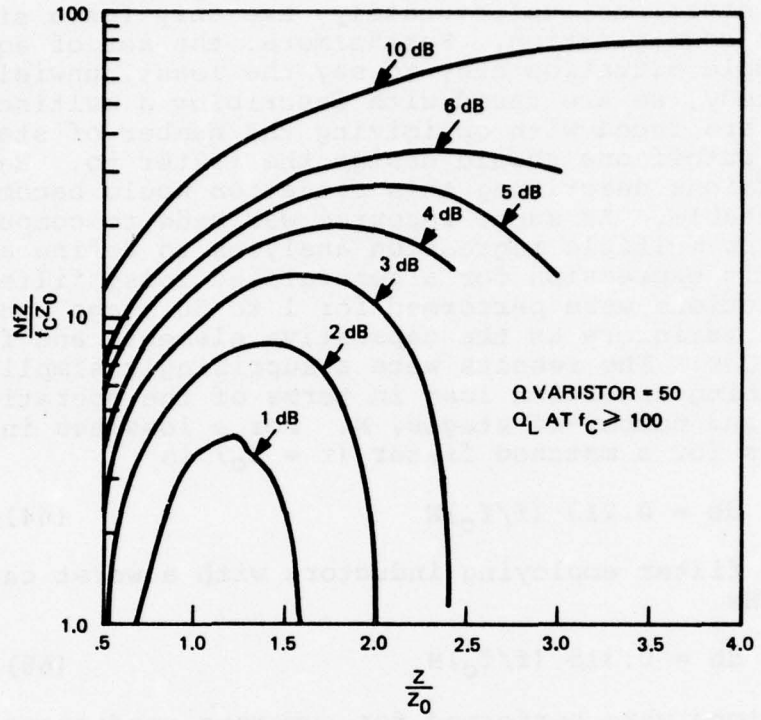


Figure 28. Optimum Termination Impedance to Yield Maximum Varistor Area to Thickness Capability for a Multi-Section Constant-K Varistor Filter (Inductor Q > 100 at 100 Megahertz, Varistor Q = 50).

$$\frac{A_T}{X_S} = \left(N \frac{f}{f_c} \frac{Z}{Z_o} \right) \frac{1}{\pi f Z \varepsilon_r \varepsilon_o} \qquad (67)$$

Note that f is fixed, being 100 MHz in the present program goal, as is Z, which is 50 ohms. Similary, ε_r is a fixed characteristic value for particular material types. As such, we can write

$$\frac{A_T}{X_S} \sim N \frac{f}{f_c} \frac{Z}{Z_o} \qquad (68)$$

3.2.3 Lumped Parameter Analysis Summary

The lumped parameter analysis has shown that high frequency, metal oxide varistor terminal protection assemblies are feasible utilizing meaningful amounts of varistor material and practical size inductive elements. A parametric configuration analysis was performed which showed the Chebyshev low pass configuration to be the most efficient with respect to maximizing the amount of varistor material which can be utilized with the Constant-K configuration being somewhat less efficient although extremely attractive from a fabrication standpoint. Detailed parametric design equations were developed for the Constant-K filter using microstrip inductors. It was shown that minimum insertion loss resulted when using a mismatched filter which also maximized the amount of varistor material in the filter. Design relationships describing the optimum filter characteristic impedance to meet specified insertion loss requirements were also developed.

3.3 Insertion Loss Comparison of Distributed and Lumped Parameter Configurations

Both the distributed and lumped parameter analyses have shown that high frequency, metal oxide varistor terminal protection devices are feasible. Both analyses have identified the varistor dielectric resistivity as the prime source of insertion loss. The distributed parameter analysis identified a modified microstrip configuration utilizing ferrites as an optimum candidate configuration. The lumped parameter analysis identified a Chebyshev configuration as the optimum, although the detailed design analyses were developed for a Constant-K filter with microstrip inductors due to its simplicity of fabrication. In selecting whether a distributed or lumped parameter configuration should be used, the selection criterion simply reduces to "what are the relative losses associated with each configuration?".

For the distributed parameter microstrip/ferrite configuration, the dielectric loss of the varistor is given by (17) as

$$db = 8.686 \frac{\ell \pi \tan \delta}{\lambda_o} \sqrt{\varepsilon_r \mu_r} \qquad (17)$$

where

ℓ = microstrip length

λ_o = wavelength in vacuum

cotan δ = varistor Q

ε_r = 875 at 100 MHz

μ_r = 1

The total varistor area, A_T, in the microstrip is related to the microstrip length, ℓ, and microstrip width, W, by

$$A_T = W\ell \qquad (69)$$

From (7)

$$\frac{W}{x} = \frac{120 \pi}{Z_o \sqrt{\varepsilon_r}} \qquad (70)$$

Thus

$$\ell = \frac{A_T Z_o \sqrt{\varepsilon_r}}{120 \pi x} \qquad (71)$$

Substituting (71) into (17) yields

$$db = \frac{0.0725 Z_o \varepsilon_r A_T}{Q \lambda_o x} \qquad (72)$$

For a 50 ohm configuration operating at 100 MHz this reduces to

$$db = 0.218 \frac{A_T}{x} \qquad (73)$$

The dielectric loss in a Constant-K filter is given by (64) as

$$db = 0.213 (f/f_c)N \qquad (64)$$

The total amount of varistor material in an N stage filter is given in (66) as

$$\frac{A_T}{x} = \frac{N}{\pi f_c Z_o \varepsilon_r \varepsilon_o} \tag{66}$$

solving for N in (66) and substituting in (64) yields

$$db = 0.213 \pi f Z_o \varepsilon_r \varepsilon_o \frac{A_T}{x} \tag{74}$$

which, for a 50 ohm filter operating at 100 MHz, reduces to

$$db = 0.258 \frac{A_T}{x} \tag{75}$$

Thus, in comparing (73) and (75) one finds that the dielectric losses in either configuration are comparable.

The conductor losses associated with each configuration have been shown to be less than the dielectric losses. Since the conductor losses are associated with the amount of conductor material present in each configuration, a relative evaluation can be obtained by examining their low frequency losses.

For the distributed parameter configuration, a conductor of width, W_D, thickness, t, and length, ℓ, is placed above the varistor material at a heigth, x,to form the microstrip configuration. For a material of resistivity, ρ, the conductor resistance, R_D, is given by

$$R_D = \frac{\rho \ell}{W_D t} \tag{76}$$

Substituting for ℓ and W using (70) and (71) yields

$$R_D = \frac{\rho A_T}{t} \left(\frac{Z_o \sqrt{\varepsilon_r}}{120 \pi x} \right)^2 \tag{77}$$

For the lumped parameter configuration, N, stages of inductors of width, W_L, thickness, t, and length, ℓ, are used to form the filter. The total filter conductor resistance, R_L, is then given by

$$R_L = \frac{N \rho \ell}{W_L t} \tag{78}$$

The required inductance per stage is given by (59) as

$$L_S = \left(Z_o\right)^2 \quad \varepsilon_r \, \varepsilon_o \, \frac{A_s}{x} \tag{59}$$

From Figure 29 the inductance of the flat ribbon can be approximated by

$$L \text{ (henries)} \sim 10^{-8} \, \ell \text{ (cm)} \tag{79}$$

Thus

$$R_L = \frac{10^8 \, \rho \, (Z_o)^2 \, \varepsilon_r \, \varepsilon_o \, N \frac{A_s}{x}}{W_L \, t} \tag{80}$$

Recalling that

$$\frac{A_T}{x} = \frac{NA_s}{x} \tag{81}$$

yields

$$R_L = \frac{10^8 \, \rho \, (Z_o)^2 \, \varepsilon_r \, \varepsilon_o \quad \frac{A_T}{x}}{W_L \, t} \tag{82}$$

The relative conductor loss between the two configurations is then obtained from (77) and (82) and is given by

$$\frac{R_L}{R_D} = \frac{1.26 \, x}{W_L} \tag{83}$$

Typical varistor thicknesses and ribbon widths which would be employed are on the order of 1 millimeter. Hence, the conductor loss ratio is on the order of 1.26 and, again, both configurations would be comparable.

4. Prototype Design and Evaluation

The insertion loss analysis presented in Section 3.3 showed that the inherent losses in the distributed and lumped parameter configurations were comparable, and were primarily associated with the dielectric resistivity of the varistor material. Since there was no overwhelming performance advantage associated with the distributed parameter approach, the lumped parameter Constant-K filter approach was chosen for prototype development in light of its simpler fabrication process.

The design characteristics given in Figure 28 indicate that for an insertion loss of 1 db, the optimum amount of varistor area is obtained at

$$\frac{Z}{Z_o} = 1.2 \tag{84}$$

$$\frac{N\ f\ Z}{f_c\ Z_o} = 4.1 \tag{85}$$

The filter termination impedance, Z, is the impedance of the system to be protected which, in the present study, is 50 ohms, Hence, the optimum filter impedance, Z_o, is

$$Z_o = 41.66 \text{ ohms} \tag{86}$$

If the maximum desirable operating frequency is established below cutoff at

$$f = 0.7\ f_c \tag{87}$$

Then the required number of filter stages is found from (85) and is

$$N = \frac{4.1}{1.2 \times 0.7} = 4.88 \sim 5 \tag{88}$$

Hence, the optimum design is a 5 stage filter with 41.66 ohms characteristic impedance operating at a maximum frequency of 0.7 f_c.

In our present case, the maximum operating frequency is 100 MHz. Hence

$$f_c = \frac{100}{0.7} = 143 \text{ MHz} \tag{89}$$

From (57) the inductance per stage is

$$L_s = 93 \text{ nanohenries} \tag{90}$$

and, from Figure 25, can be obtained using a 1 mil thick, 30 mil wide ribbon of 3.2 inches long.

From (56) and (58), the capacitance per stage is

$$C_s = 53.5 \text{ picofarads} \tag{91}$$

$$\frac{A_s}{x} = 0.691 \text{ centimeters} \tag{92}$$

while the total capacitance for the 5 stage filter is

$$C_T = 267.5 \text{ picofarads} \tag{93}$$

$$\frac{A_T}{x} = 3.45 \text{ centimeters} \tag{94}$$

The total varistor area to thickness ratio of 3.45 compares favorably with the maximum capability of 4.9 given in Figure 3.

Figure 29 shows the schematic diagram of the prototype filter which was developed from the preceeding design procedure. The analytical insertion loss of the filter is shown in Figure 30, together with the insertion loss associated with a single varistor unit of the same total capacitance. Figure 31 shows that the analytical phase shift associated with the filter is nearly linear over the frequency band of interest. For a distortionless system, the phase shift must be zero or must vary linearly with frequency as "-kf" where K is a positive constant (Reference 23). Furthermore, the delay time, t_d, through the filter is given by

$$t_d = -\frac{d\phi}{df} = \frac{\Delta\phi \text{ (degrees)}}{360 \times \Delta f \text{ (Hertz)}} \tag{95}$$

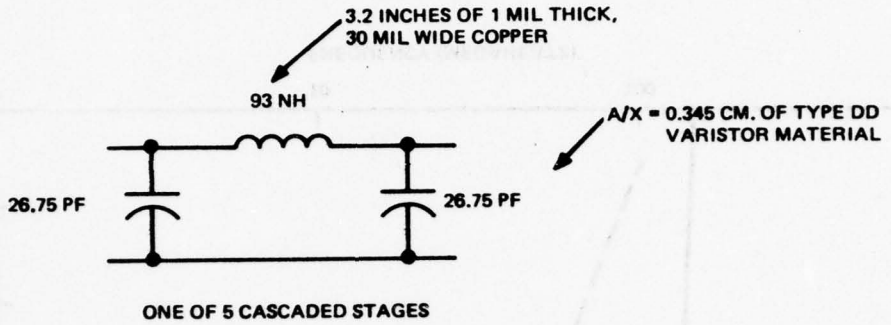


Figure 29. Single π Section of the Prototype Five Stage Constant-K Varistor Filter.

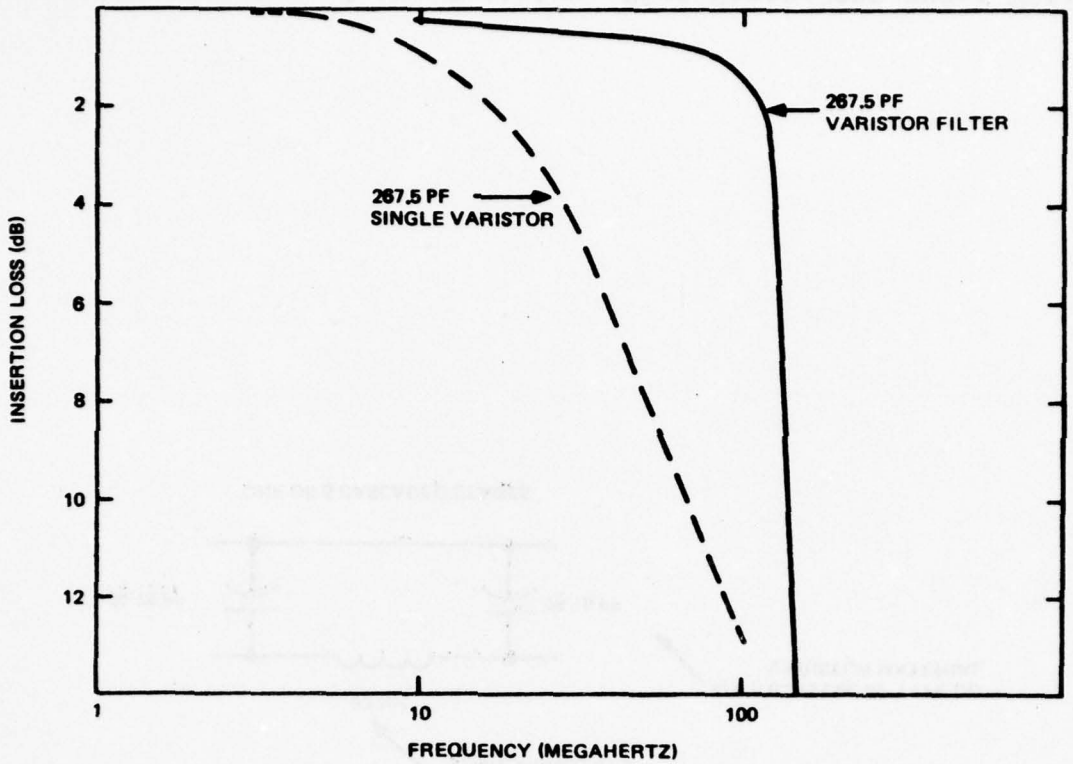


Figure 30. Design Insertion Loss of the Prototype Five Stage Constant-K Varistor Filter.

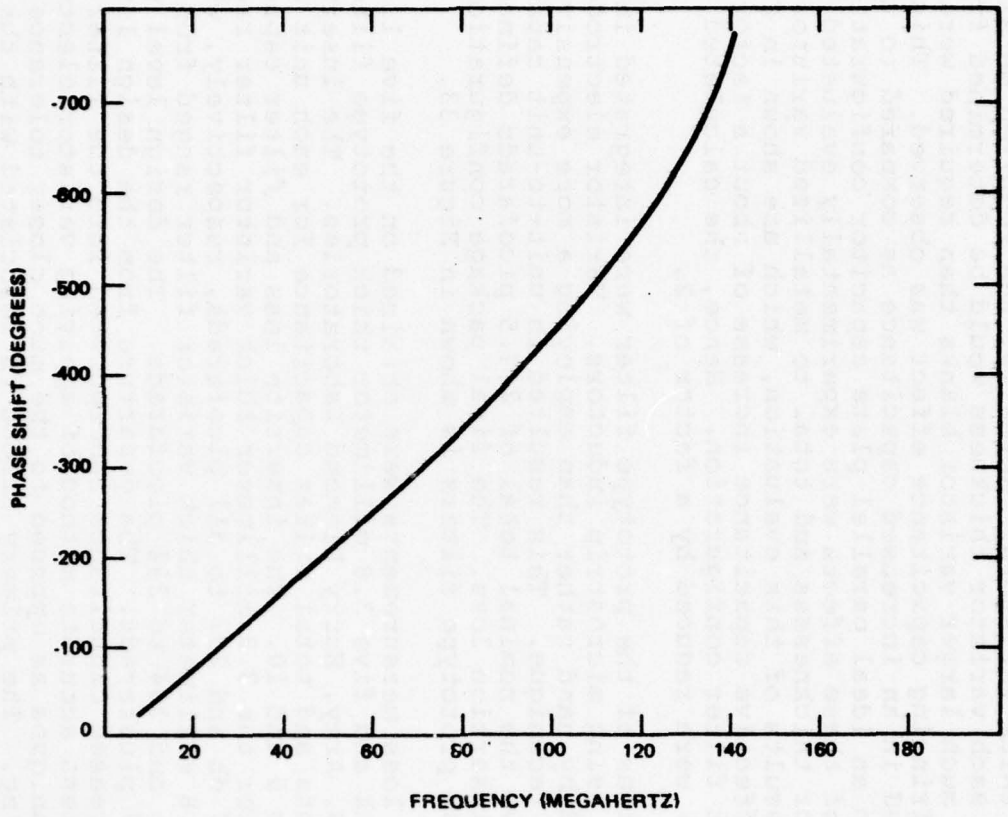


Figure 31. Design Phase Shift of the Prototype Five Stage Constant-K Varistor Filter.

Which, for the characteristics shown in Figure 31, yield

$$t_d = 12.3 \text{ nanoseconds} \qquad (96)$$

The prototype filter was fabricated using standard 6.5 millimeter diameter unmetallized Type DD varistor blanks obtained from the General Electric Company, Semiconductor Products Department. Two filter versions were fabricated for evaluation. One type utilized 1.8 millimeter thick varistors while the other used 3.8 millimeter thick varistors. Normally, the required metallization areas for each varistor thickness would be determined from (92). However, since much larger varistor blanks than required were used, a significant fringing capacitance effect was observed. This, in effect, resulted in an increased capacitance as compared to that calculated from an ideal parallel plate capacitor configuration. The magnitude of these effects were experimentally evaluated using various varistor thicknesses and total to metallized varistor area ratios. The results of this evaluation, which are shown in Figure 32, indicated an effective capacitance increase of about a factor of 2 for the present filter configuration. Hence, the calculated varistor areas from (92) were reduced by a factor of 2.

Both versions of the prototype filter were integrated into a planar package using microstrip inductors. Varistor electrode areas were fabricated by hand rather than employing a more expensive silk screening technique. This resulted in unit-to-unit capacitance variations above the nominal total of 267.5 picofarads defined in (93) for 1 db insertion loss. The final package configuration provided for the prototype filters is shown in Figure 33.

Insertion loss measurements were obtained on the five 1.8 millimeter thick and five 3.8 millimeter thick prototype filters provided to U.S. Army, Harry Diamond Laboratories. The insertion loss measurements and total filter capacitance for each unit are shown in Tables 9 and 10. The insertion loss and filter capacitance results for the 3.8 millimeter thick varistor filter ranged from 1.6 to 2.7 db and 293 to 311 picofarads, respectively, while that for the 1.8 millimeter thick varistor filter ranged from 3.40 to 4.00 db and 304 to 344 picofarads. The design level was 1.39 db and 267 picofarads. The departure from the design level is due to the increased capacitance incorporated into the filter as a result of the less accurate method of applying varistor electrodes using hand techniques as opposed to the much closer tolerance method of silk screening. The primary effect is associated with the stage to stage variation rather than a uniform increase in total filter capacitance. This stage to stage variation is manifested by the small resonances throughout the passband as compared to the monotonically decreasing insertion loss for the uniform lossy filter design. In spite of this, the results are extremely encouraging and do demonstrate that the filter approach is a viable method of integrating the metal oxide varistor into high frequency systems.

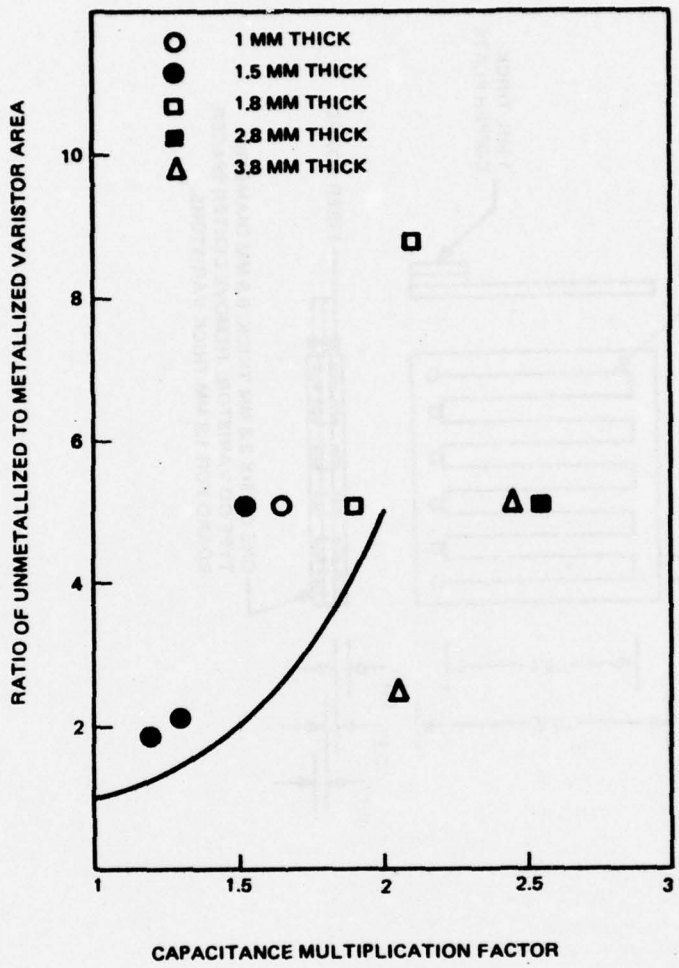


Figure 32. Fringing Capacitance Effects in Various Metal Oxide Varistor Material Geometries.

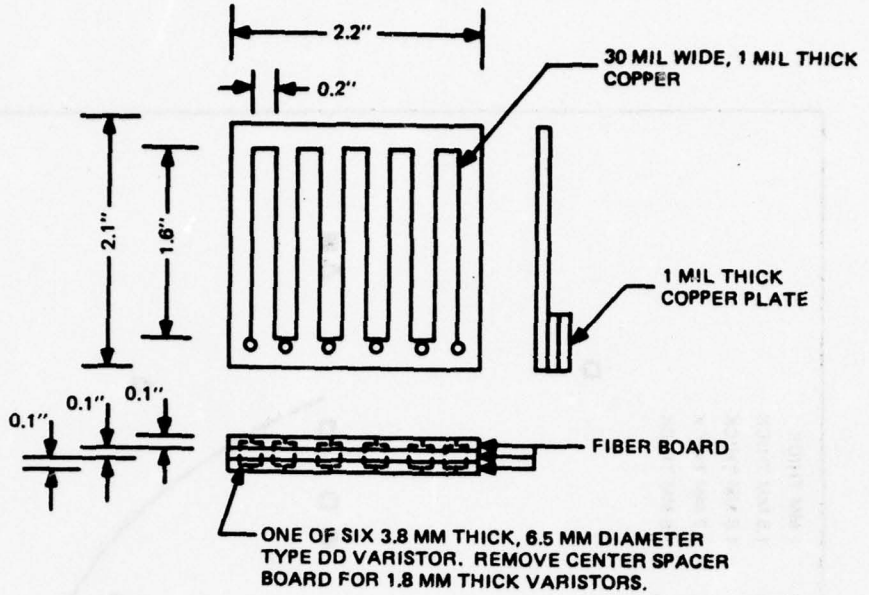


Figure 33. Engineering Assembly Drawing of the Prototype Five Stage Constant-K Varistor Filter.

TABLE 9. Insertion Loss Characteristics of the 3.8 Millimeter Thick, Metal Oxide Varistor Filters

FREQUENCY MHz	INSERTION LOSS (db) MODEL 267pf	SN 01 299pf	SN 02 296pf	SN 03 293pf	SN 04 311pf	SN 05 282pf
10	0.21	0.94	0.57	0.60	0.72	0.34
20	0.38	1.20	1.30	1.10	1.30	0.93
30	0.44	1.40	1.50	1.50	1.50	1.00
40	0.47	1.10	1.10	1.00	1.40	1.00
50	0.58	0.94	0.82	0.87	0.77	0.83
60	0.70	0.94	1.00	0.87	0.89	0.98
70	0.80	1.90	1.90	1.90	2.00	2.00
80	0.93	1.60	1.90	1.90	1.80	2.10
90	1.10	0.90	1.30	1.40	1.30	2.30
100	1.39	1.60	1.80	1.80	1.70	2.70

TABLE 10. Insertion Loss Characteristics of the 1.8 Millimeter Thick, Metal Oxide Varistor Filters.

FREQUENCY MHz	INSERTION LOSS (db)					
	MODEL 267pf	SN 06 340pf	SN 07 328pf	SN 08 344pf	SN 09 334pf	SN 10 304pf
10	0.21	1.10	0.78	0.92	0.67	0.64
20	0.38	1.80	1.50	1.90	1.40	1.50
30	0.44	2.10	1.90	1.90	1.70	1.60
40	0.47	1.80	1.90	1.90	1.70	1.60
50	0.58	1.60	1.90	1.60	1.60	1.60
60	0.70	2.00	1.90	2.20	1.90	2.20
70	0.80	2.90	2.50	3.40	2.60	3.00
80	0.93	3.10	2.70	3.80	2.30	3.60
90	1.10	3.40	2.90	3.40	3.00	3.40
100	1.39	4.00	3.40	4.00	3.80	3.90

This is particularly significant since it must be kept in mind that the program objective was not to develop optimum fabrication techniques, but to demonstrate the feasibility of the integration concept. As such, insertion loss and size can be decreased by using multilayer connnections for spiraled inductors to optimize inductor size and employing silk screening techniques for accurate varistor electroding.

Engineering versions of each filter type were also fabricated for evaluation under high current pulse stressing. Both the 1.8 millimeter and 3.8 millimeter thick varistor filters were exposed to 15 microsecond wide critically damped pulses. Both the total filter current and filter output voltage when terminated in 50 ohms were monitored. The essential results of these tests are given in Table 11. Shown here are peak pulse voltage and peak pulse current that was exhibited by each filter type along with the calculated peak voltage value using the material characteristics given in Table 1. The close agreement of the experimental and calculated values shows that the varistor characteristics are preserved even when integrated into the filter configuration.

TABLE 11. Typical High Pulse Power Voltage-Current Characteristics of the Five Stage Constant-K Varistor Filters.

THICKNESS (MM)	* AREA (CM^2)	V PEAK (VOLTS)	I PEAK (AMPERES)	V CALCULATED
1.8	0.76	530	90	500
		670	280	590
		970	1100	760
		1200	2500	900
3.8	1.44	900	90	990
		1000	270	1100
		1200	780	1300
		1500	2500	1600

* Effective Area Calculated From Total Filter Capacitance

5. Advanced Metal Oxide Varistor Material Considerations

Although the detailed analyses, design and development of the varistor terminal protection device involved the more extensively characterized Type DD material, a moderate level subtask of the program was concerned with evaluating the potential application of a new class of General Electric Company developed varistor materials. The two primary material types of concern were a thick film metal oxide varistor material and the presently so-called "reconstituted" metal oxide varistor material. Both material types are still in the developmental stages within the General Electric Company. However, they do appear attractive for high frequency terminal protection applications, particularly the "reconstituted" material. In view of their potential application, a number of samples of each type were fabricated by the General Electric Research and Development Center and supplied to the Space Division for evaluation.

The "reconstituted" varistor material consists of a powdery mixture which can be molded under moderate temperatures to any geometrical configuration desired. The interest in this material can be appreciated by examining the varistor characteristics shown in Figure 34. Shown here are the insertion losses associated with a 1 millimeter thick, 8 millimeter diameter standard sintered Type DD varistor material and the insertion loss characteristics of the same sized "reconstituted" material. As seen, the "reconstituted" material exhibits an effective dielectric constant of about a factor of thirty less than the standard sintered material. As such, the potential impact of this material to high frequency applications is obvious. The voltage-current characteristics of this material are shown in Figure 35 along with an indication of its energy absorption capability. Although the clamping voltage characteristics, admittedly, are not quite as good as the standard sintered material, it should be remembered that the "reconstituted" material is a comparative infant with respect to its development cycle.

One of the most attractive applications for the "reconstituted" material, in light of the present studies, is obviously with respect to the distributed parameter microstrip configuration. The material, though, would also be attractive for use in the lumped parameter filter approach, whereby it could be utilized as the filter substrate as well as the active capacitance element.

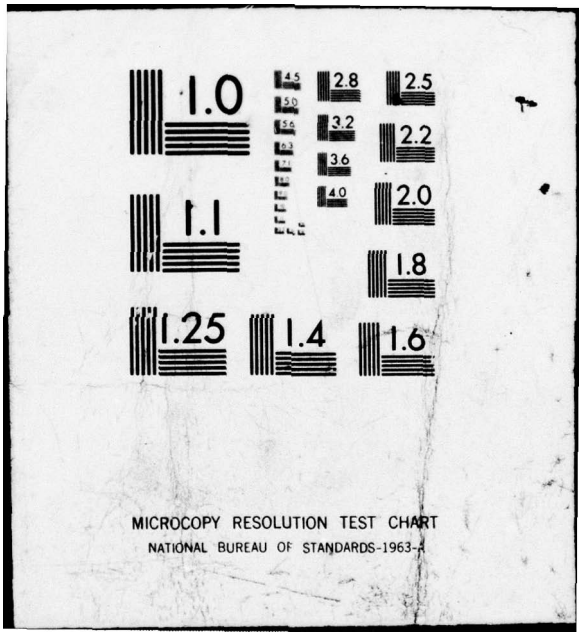
The other advanced varistor material type evaluated was the thick film type. This material, as its name implies, can be applied using standard thick film techniques and has potential interest in high frequency, thick film device technology. The thick film varistor material, however, is somewhat younger in development life cycle as compared to the "reconstituted" material. The voltage-current characteristics of a 0.18 millimeter thick, 10 millimeter diameter material sample are shown in Figure 36. Also shown is an indication of the energy absorption capability of this material.

AD-A033 785 GENERAL ELECTRIC CO PHILADELPHIA PA SPACE DIV F/G 9/5
EMP SURGE SUPPRESSION DEVICES UTILIZING METAL OXIDE VARISTORS F--ETC(U)
MAR 76 D M TASCA, S J STOKES, J P QUINE DAAG39-75-C-0008
UNCLASSIFIED 755DS-4272 HDL-CR-76-008-1 NL

2 OF 2
AD
A033785



END
DATE
FILMED
2-77


1.0
1.1
1.25
1.4
1.6
1.8
2.0
2.2
2.5
2.8
3.2
3.6
4.0
4.5
5.0
MICROCOPY RESOLUTION TEST CHART
NATIONAL BUREAU OF STANDARDS-1963-A

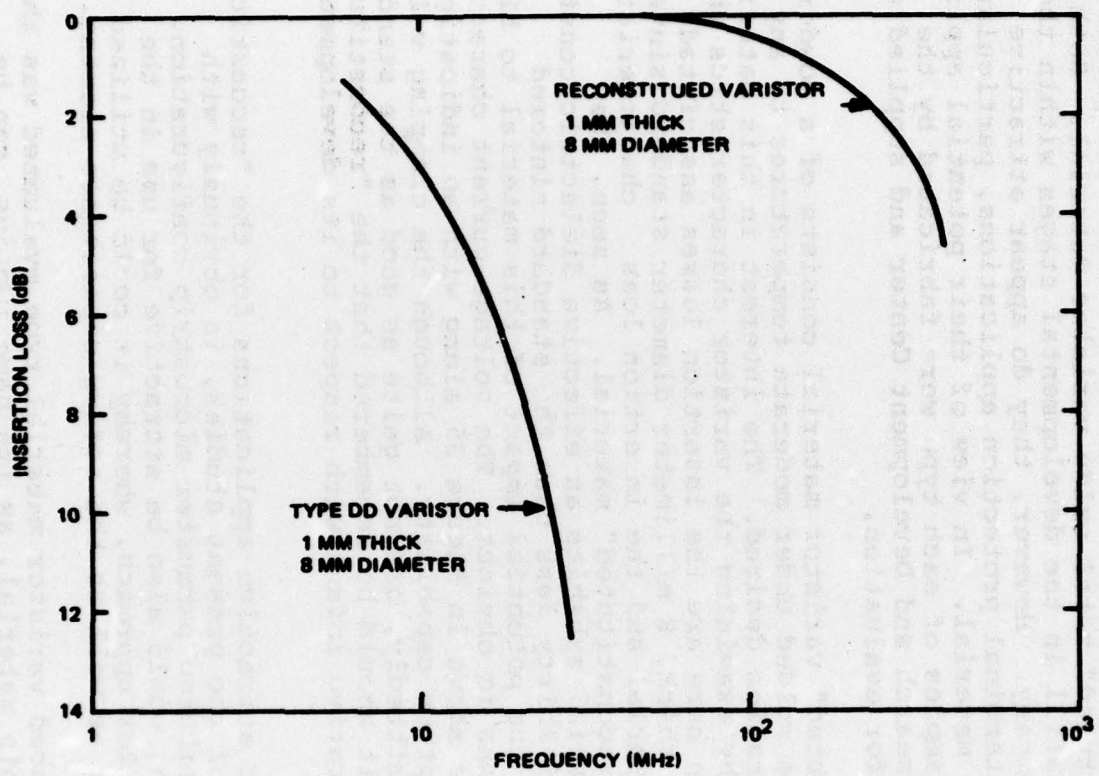


Figure 34. Insertion Loss Characteristics of Standard Sintered & "Reconstituted" Metal Oxide Varistor Materials.

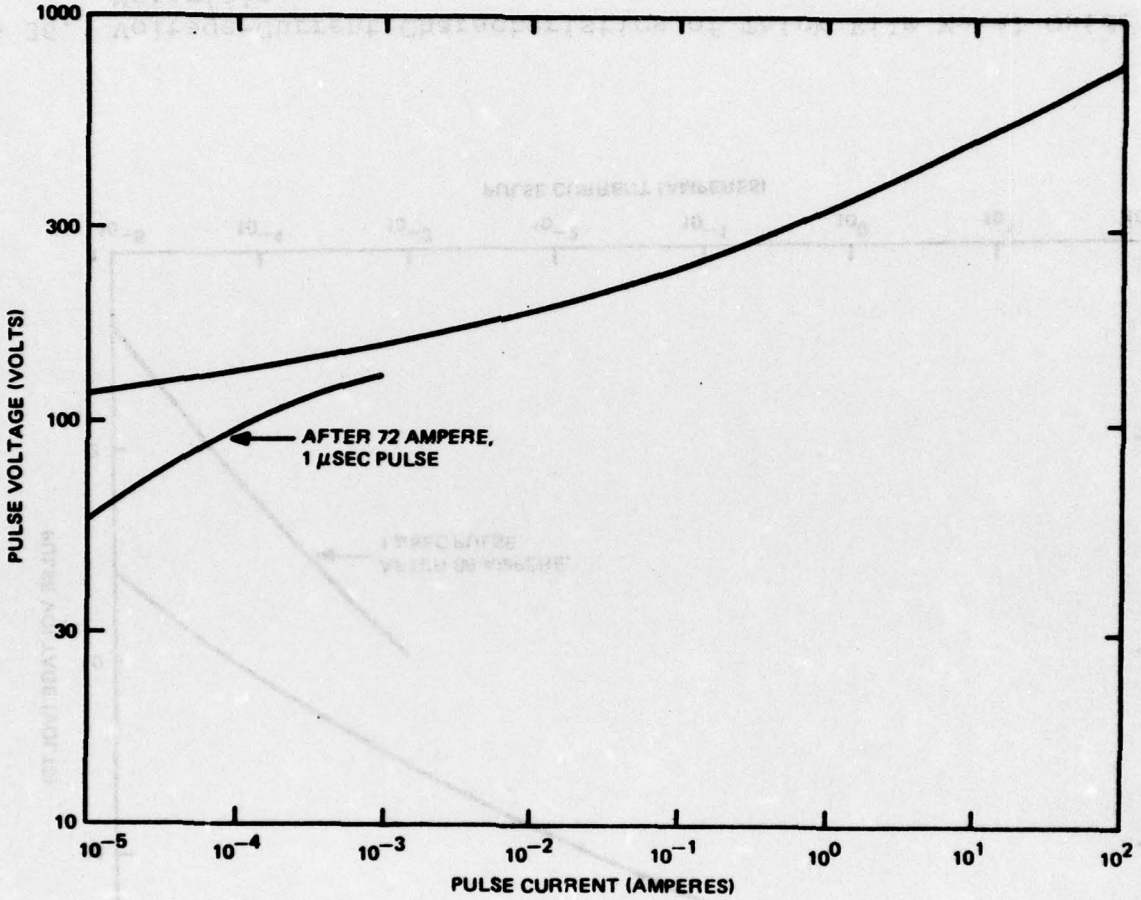


Figure 35. Voltage-Current Characteristics of "Reconstituted" Metal Oxide Varistor Materials.

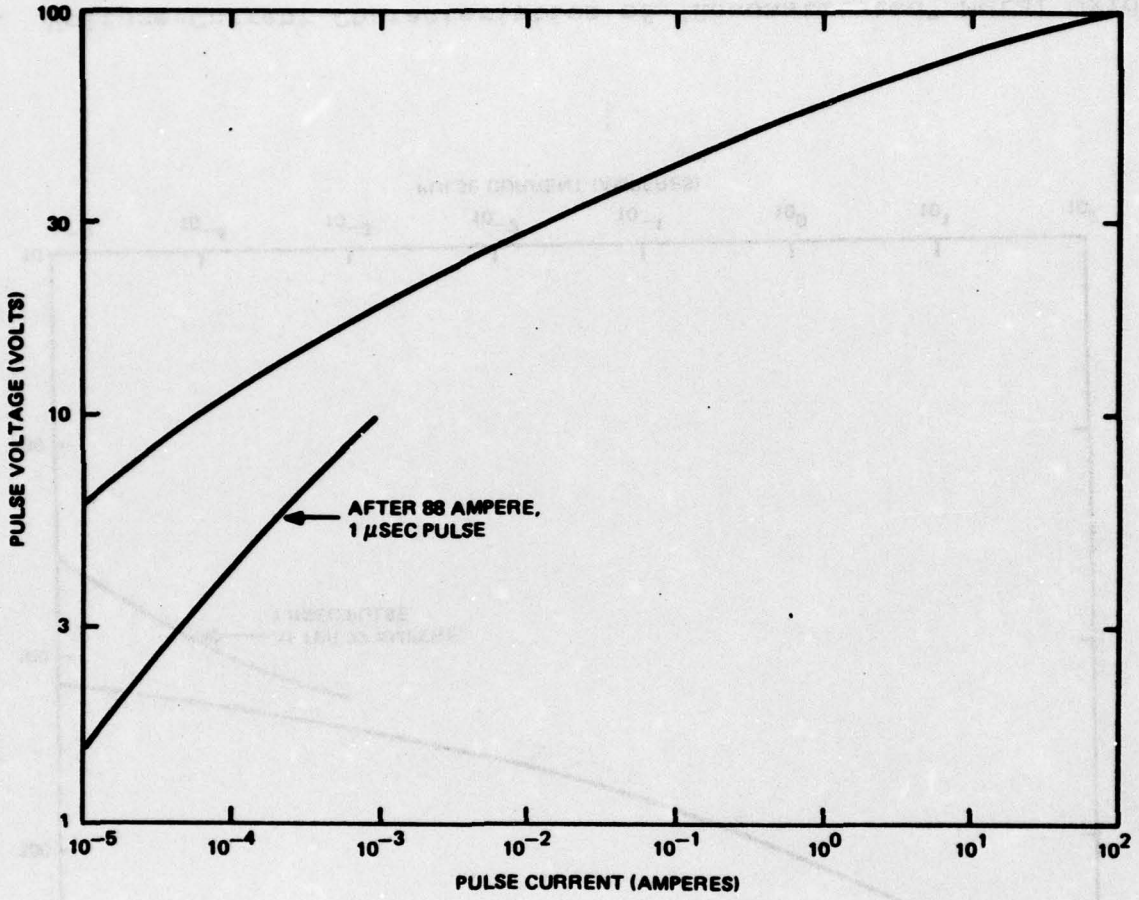


Figure 36. Voltage-Current Characteristics of Thick Film Metal Oxide Varistor Materials.

6. Conclusions

Both the distributed parameter and lumped parameter studies have shown that high frequency, metal oxide varistor terminal protection assemblies are feasible. Parametric design analyses were performed which showed that a modified microstrip line incorporating a ferrite with relative permeability of greater than 16 was an optimum configuration for a distributed parameter assembly. A similar parametric analysis showed that low pass Chebyshev and Constant-K filter configurations represented the optimum for a lumped parameter assembly.

Insertion loss analyses for both the distributed parameter and lumped parameter configurations identified the dielectric resistivity of the metal oxide varistor as the prime source of insertion loss. A comparison of losses between both configurations also showed that the inherent losses in the distributed and lumped parameter configurations were comparable. Since there was no overwhelming performance advantage associated with the distributed parameter approach, the lumped parameter Constant-K filter approach was chosen for prototype development in light of its simpler fabrication process.

Detailed design equations were developed for a Constant-K filter with microstrip inductors as the baseline configuration. A significant result was the development of a parametric relationship which showed that for any given allowable insertion loss, a particular mismatched filter represented the optimum design which minimized the insertion loss and maximized the amount of varistor material capable of being integrated into the filter assembly.

Two prototype filter versions based on this optimum design were developed and fabricated for evaluation. One version utilized 1.8 millimeter thick varistor elements while the other utilized 3.8 millimeter thick varistor elements. The design insertion loss and total filter capacitance was 1.39 db and 267 picofarads. The 1.8 millimeter thick units were measured to be in the range of 3.4 to 4 db and 304 to 344 picofarads, respectively. The 3.8 millimeter thick units were measured to be in the range of 1.6 to 2.7 db and 293 to 311 picofarads. The departure from the design level was not due to the varistor integration concept, but was a result of the increased capacitance incorporated into the filter due to the method used in fabricating the varistor electrodes. For the prototype units, varistor electrodes were fabricated using hand techniques as opposed to the much closer tolerance method of silk screening.

Engineering versions of each filter type were also fabricated for evaluation under high current pulse stressing. Both the 1.8 millimeter and 3.8 millimeter thick varistor filters were exposed to 15 microsecond wide critically damped pulses of 100 to 2500 amperes peak level. The filter output voltage was measured and

compared to calculated values using the previously known material characteristics. The close agreement of the experimental and calculated values demonstrated that the varistor characteristics are preserved even when integrated into the filter configuration.

Some basic performance information on advanced varistor material compositions was also obtained. The material types examined were a thick film metal oxide varistor material and the presently so-called "reconstituted" metal oxide varistor material. Both material types are still in the developmental stages within the General Electric Company. However, they do appear attractive for high frequency terminal protection applications. The "reconstituted" varistor material consists of a powdery mixture which can be molded under moderate temperatures to any geometrical configuration desired. The material exhibits an effective dielectric constant of about a factor of thirty less than the standard sintered material and is attractive for applications as a microstrip or filter substrate. The thick film varistor material, as its name implies, can be applied using standard thick film techniques and has potential interest in high frequency, thick film device technology.

7. Recommendations

The present program has shown that the metal oxide varistor material can be readily integrated into a high frequency assembly using either a distributed parameter microstrip configuration or a lumped parameter filter configuration. However, in order to develop these devices into practical hardening tools covering the widest possible range of applications, more work in the following areas is needed.

The primary effort should be with respect to developing optimum package configurations to reduce both stray capacitance and overall assembly size. Existing technology, such as, multilayer hybrid techniques to reduce inductor size and increase inductor efficiency should be pursued. Other techniques such as utilizing a varistor slab as the filter substrate with screened-on inductors should also be evaluated. Also of interest would be configurations such as a tuneable slug filter, in either a Chebyshev or Constant-K version, in which the varistor is the tuneable element. Additional work in developing a microstrip/ferrite or coaxial helical transmission line configuration should also be pursued.

More work should definitely be done in characterizing both the "reconstituted" and thick film varistor materials and applying them in high frequency applications. The "reconstituted" material, by virtue of its much lower effective dielectric constant, is extremely attractive for applications in microstrip confiqurations. Similarly, the thick film varistor material has potential application in high frequency, thick film device technology.

8. References

1. Tasca, D.M. and Peden, J.C., "EMP Surge Suppression Connectors Utilizing Metal Oxide Varistors", Final Technical Report, Contract No. DAAG39-72-C-0179, General Electric Report 73SD4293, December 1973, U.S. Army Harry Diamond Laboratory Report No. HDL-TR-179-1, August 1974.

2. Levinson, L. M. and Philip, H.R., "AC Properties of Metal Oxide Varistors", General Electric Report 75CRD175, September 1975.

3. Levinson, L. M. and Philipp, H. R., "Metal Oxide Varistor--A Multijunction Thin-Film Device", General Electric Company Report 73CRD285, October 1973.

4. Schneider, M. V., "Microstrip Lines for Microwave Integrated Circuits", Bell System Technical Journal, May-June 1969, pp. 1421-1444.

5. Quine, J. P., Tomiyasu, K., and Younger, C., "Pulse Modulations of Gallium Arsenide Injection Luminescent Diode Laser", Proc. IEEE, Vol. 51, p. 1141, August 1963.

6. Winkler, M.R.,and Kollman, H., "Discussion on High Impedance Cable", Proc. IRE, October 1947, pp. 1097-1100.

7. Kollman, H.E., "High-Impedance Cable", Proc. IRE, June 1946, pp. 348-351.

8. Sickak, W., "Coaxial Line with Helical Inner Conductor", Proc. IRE, August 1954, pp. 1315-1319.

9. Zverev, A. I., "Handbook of Filter Synthesis", John Wylie & Sons, 1967.

10. Hilburn, J. L. and Johnson, D. E., "Manual of Active Filter Design", McGraw-Hill Book Company, 1973.

11. Lewis, I. A. D. and Wells, F. H., "Millimicrosecond Pulse Techniques", Pergamon Press, 1959.

12. Presser, A., "RF Properties of Microstrip Line", Microwaves, March 1968.

13. Schilling, W. and Lehrfeld, S., The Real World of Micromin Substrates", Microwaves, Part 1 - December 1968; Part 2 - January 1969; Part 3 - March 1969; Part 4 - September 1969.

14. Caulton, M., et al, "UHF Film Integrated Circuits", AD 864090.

15. Daly, A.D., Knight, S.P., and Caulton, M., "Lumped Elements in Microwave Integrated Circuits", IEEE Transactions on Microwave Theory and Techniques, Vol. MTT-15, #12, December 1967.

16. Sobol, H., "Technology and Design of Hybrid Microwave Integrated Circuits", Solid State Technology, February 1970.

17. "Reference Data for Radio Engineers", Section 20 - Microminiature Electronics, Howard Sams & Company, Incorporated, 5th Edition, March 1970.

18. Caulton, M., "The Lumped Element Approach to Microwave Integrated Circuits", The Microwave Journal, May 1970.

19. Harper, C. A., "Handbook of Thick Film Hybrid Microelectronics", McGraw-Hill Book Company.

20. Terman, F. E., "Radio Engineers Handbook", McGraw-Hill Book Company, 1943 Edition.

21. Caulton, M., Knight, S. P. and Daly, D. A., "Hybrid Integrated Lumped-Element Microwave Amplifiers", IEEE Transactions on Electron Devices, Vol. ED-15, #7, July 1968.

22. Giacoletto, L. J., "Optimum Resistive Terminations for Single Section Constant-K Ladder Type Filters", RCA Review, September 1947.

23. Chirlian, P. M., "Electronic Circuits: Physical Principles, Analysis and Design", McGraw-Hill Book Company, 1971.